The k-j-j' vector correlation in inelastic and reactive scattering.

M. Brouard,[1, a)] H. Chadwick,[1] C. J. Eyles,[1] F. J. Aoiz,[2, b)] and J. Kłos[3, c)]

[1)] *The Department of Chemistry, University of Oxford, The Physical and Theoretical Chemistry Laboratory, South Parks Road, Oxford, OX1 3QZ, United Kingdom.*

[2)] *Departamento de Química Física, Facultad de Química, Universidad Complutense, 28040 Madrid, Spain*

[3)] *Department of Chemistry and Biochemistry, University of Maryland, College Park, MD, 20742, USA*

(Dated: 21 July 2011)

Quasi-classical trajectory (QCT) methods are presented which allow characterization of the angular momentum depolarization of the products of inelastic and reactive scattering. The particular emphasis of the theory is on three-vector correlations, and on the connection with the two-vector correlation between the initial and final angular momenta, $\boldsymbol{j}$ and $\boldsymbol{j}'$, which is amenable to experimental measurement. The formal classical theory is presented, and computational results for NO(A) + He are used to illustrate the type of mechanistic information provided by analysis of the two- and three-vector correlations. The classical $\boldsymbol{j}$-$\boldsymbol{j}'$ two-vector correlation results are compared with quantum mechanical calculations, and are shown to be in good agreement. The data for NO(A) + He support previous conclusions [J. Chem. Phys. **131**, 104307, (2009)] that this system is only weakly depolarizing. Furthermore, it is shown that the projection of $\boldsymbol{j}$ along the kinematic apse is nearly conserved for this system under thermal collision energy conditions.

[a)]Electronic mail: mark.brouard@chem.ox.ac.uk

[b)]Electronic mail: aoiz@quim.ucm.es

[c)]Electronic mail: jklos@umd.edu

I. INTRODUCTION

Collisional processes are inherently anisotropic, and therefore for a full understanding of the dynamics of these scattering events it is necessary to consider the vector properties of the system. The stereodynamics of a collision between a closed shell atom and a diatom is completely defined by four vectors, $\boldsymbol{k}$, $\boldsymbol{k}'$, $\boldsymbol{j}$ and $\boldsymbol{j}'$, where $\boldsymbol{k}$ and $\boldsymbol{k}'$ are the initial and final relative velocity vectors, and $\boldsymbol{j}$ and $\boldsymbol{j}'$ are the initial and final rotational angular momenta of the molecule[1–6]. Lower order vector correlations can be obtained by integrating over the directions of one or more of the vectors. For example, the $\boldsymbol{k}$-$\boldsymbol{k}'$-$\boldsymbol{j}'$ distribution is obtained by integrating over all possible directions of $\boldsymbol{j}$[7–10]. The differential cross section (which quantifies the $\boldsymbol{k}$-$\boldsymbol{k}'$ correlation) can be obtained from the three-vector correlation by integrating over all possible directions of $\boldsymbol{j}'$. Analogously, integrating the initial four vector correlation over all possible directions of $\boldsymbol{k}$ and $\boldsymbol{k}'$ leads to the $\boldsymbol{j}$-$\boldsymbol{j}'$ correlation.

The two-vector $\boldsymbol{j}$-$\boldsymbol{j}'$ correlation, sometimes referred to as the rotational tilt, has been the focus of much recent experimental and theoretical attention. Our studies have been mainly concerned with the collisional depolarization of electronically excited $^2\Sigma^+$ radicals, including OH(A) with H_2O[11] and Ar[12–16], and NO(A) with He and Ar[17], which we have probed using Zeeman and hyperfine quantum beat spectroscopy techniques. This work has been complemented by studies from McKendrick and coworkers, who have used polarization spectroscopy to interrogate the collisional depolarization of OH(X), OH(A), and CN(A) with a range of collision partners[16,18–25]. On the theoretical side there has been considerable recent progress made on understanding the dynamics of elastic depolarization through the work of Dagdigian and Alexander on the collisions of OH(X) with Ar[26] and He[27], and NO(X) + Ar[28]. This work has been extended very recently by Ma *et al.* to the collisional depolarization of $CH_2(\tilde{a})$ by He[29].

In the following we develop the necessary machinery to calculate the $\boldsymbol{k}$-$\boldsymbol{j}$-$\boldsymbol{j}'$ distribution using quasi-classical trajectory (QCT) methods, and show how it reduces to the well-known expressions for the $\boldsymbol{j}$-$\boldsymbol{j}'$ vector correlation which is more amenable to experimental measurement. We show how these calculations can be extended to the $\boldsymbol{a}$-$\boldsymbol{j}$-$\boldsymbol{j}'$ vector correlation, in which $\boldsymbol{a}$ represents the kinematic apse. The kinematic apse for inelastic scattering is defined by the following equation[30]

$$\hat{\boldsymbol{a}} = \frac{\boldsymbol{k}' - \boldsymbol{k}}{|\boldsymbol{k}' - \boldsymbol{k}|} \,. \tag{1}$$

The $\boldsymbol{a}$-$\boldsymbol{j}$-$\boldsymbol{j}'$ vector correlation is particularly illuminating because in the case of collisions between rigid bodies it is known that the projection of $\boldsymbol{j}$ along the kinematic apse must be conserved[31,32]. We illustrate the QCT methodology by reference to rotational energy transfer (RET) and depolarization collisions between NO(A) and He, which is a system largely dominated by repulsive interactions at thermal collision energies[33]. For the $\boldsymbol{j}$-$\boldsymbol{j}'$ two-vector correlation a detailed comparison is made with the results of exact closed-shell and open-shell quantum mechanical (QM) calculations. We have previously compared the results of an experimental study of collisional depolarization in this system with those from QCT theory, and shown them to be in excellent agreement[17]. Once validated in this way, the QCT approach can offer mechanistic insight into the dynamics of rotational energy transfer and collision depolarization, as illustrated in the accompanying paper (see below)[34]. It also has the potential to be used for much larger systems than are currently amenable to exact quantum mechanical calculations.

The outline of the paper is as follows. Section II describes the classical theory relevant to the description of the collisional depolarization in several frames, with a particular emphasis on the three-vector correlations between the vectors $\boldsymbol{k}$ or $\boldsymbol{a}$, $\boldsymbol{j}$ and $\boldsymbol{j}'$. Section III presents the equations necessary to describe the polarization in the laboratory (lab) frame, and provides the necessary formulae to apply the theory to analysis of experimental data. The link with the analogous QM formulae is also provided in this section. Section IV briefly presents the QCT and QM computational procedures employed. The results from the QCT calculations are shown and discussed in Section V, where they are also compared with the results of QM calculations of the $\boldsymbol{j}$-$\boldsymbol{j}'$ two-vector correlation. The final section summarizes our principal conclusions. In the accompanying paper, we use the theory developed here to explore the comparative mechanisms of RET and collisional depolarization in OH(A) and NO(A) collisions with Ar[34]. It should be emphasized that the theory developed here is general, however, and could equally be used to study the dynamics of reactive collisions.

II. VECTOR CORRELATIONS

The classical theory of the $\boldsymbol{k}$-$\boldsymbol{j}$-$\boldsymbol{j}'$ correlation presented in this section is closely related to previous work on the $\boldsymbol{k}$-$\boldsymbol{k}'$-$\boldsymbol{j}'$ and $\boldsymbol{k}$-$\boldsymbol{j}$-$\boldsymbol{k}'$ distributions[7,8,35], equations for which are not reproduced here. However, the symmetry restrictions are different in the case of the $\boldsymbol{k}$-$\boldsymbol{j}$-

$\boldsymbol{j}'$ correlation, as discussed below. The theory applies to closed shell species, for which the total rotational angular momentum of the diatomic molecule $\boldsymbol{j}$ is equivalent to the rotational angular momentum, $\boldsymbol{N}$. The extension of the theory to open shell molecules in $^2\Sigma^+$ electronic states, such as NO(A) and OH(A), has been presented previously in the literature[13], and is reviewed briefly in Section IV A. Although links with the appropriate QM expressions are provided in Section III B, the equations presented in the following section are purely classical, and do not include the Clebsch-Gordon term which appears in recent treatments of the classical-quantum correspondence limit[36,37].

A. *k-j-j′* vector correlation

1. *Bipolar moment expansion*

To consider the vector correlations presented in the following sections, it is useful to use one of the reference frames shown in Fig. 1. Fig. 1a shows the conventional $\boldsymbol{k}$-$\boldsymbol{k}'$ scattering frame, used to describe the $\boldsymbol{k}$-$\boldsymbol{k}'$-$\boldsymbol{j}'$ vector correlation, in which the initial relative velocity $\boldsymbol{k}$ is defined as lying along the z-axis, and the final relative velocity $\boldsymbol{k}'$ lies in the zx-plane. In the case of the $\boldsymbol{k}$-$\boldsymbol{j}$-$\boldsymbol{j}'$ vector correlation, it is more convenient to use the reference frame shown in Fig. 1b, in which the z-axis lies along $\boldsymbol{k}$ and $\boldsymbol{j}$ lies in the zx-plane, directed towards the $+x$-direction. We will denote this frame as the $\boldsymbol{k}$-$\boldsymbol{j}$ frame. With this choice of coordinate system, the $\boldsymbol{k}$-$\boldsymbol{j}$-$\boldsymbol{j}'$ distribution for an A + BC collision can then be expanded in a bipolar harmonic series[7]

$$P(\omega_j, \omega_{j'}) = \frac{1}{16\pi^2} \sum_{K,Q} \sum_{k_1,k_2} [k_1][k_2]\, h_Q^K(k_1 k_2)\, [B_Q^K(k_1 k_2; \omega_j, \omega_{j'})]^\star \,, \tag{2}$$

where $[n] = 2n + 1$, $\omega_j = (\theta_j, \phi_j)$, $\omega_{j'} = (\theta_{j'}, \phi_{j'})$ are the solid angles representing the directions of $\boldsymbol{j}$ and $\boldsymbol{j}'$, and $h_Q^K(k_1 k_2)$ are the bipolar moments of the correlated distribution. The (complex conjugate) bipolar harmonics are defined

$$\begin{aligned}
[B_Q^K(k_1 k_2; \omega_j, \omega_{j'})]^\star &= \sum_{q_1,q_2} (-1)^{K-Q} [K]^{1/2} \begin{pmatrix} k_1 & K & k_2 \\ q_1 & -Q & q_2 \end{pmatrix} C^\star_{k_1 q_1}(\theta_j, \phi_j)\, C^\star_{k_2 q_2}(\theta_{j'}, \phi_{j'}) \\
&= \sum_{q_1,q_2} \langle k_1 q_1, k_2 q_2 | K Q \rangle C^\star_{k_1 q_1}(\theta_j, \phi_j)\, C^\star_{k_2 q_2}(\theta_{j'}, \phi_{j'}) \,,
\end{aligned} \tag{3}$$

where $(\cdots)$ is a 3-j symbol, $\langle \cdots \rangle$ is a Clebsh-Gordon coefficient, and the $C_{kq}(\theta, \phi)$ are the modified spherical harmonics[38].

The choice of the $\boldsymbol{k}$-$\boldsymbol{j}$ plane as the reference plane implies that $\phi_j = 0$. In addition, the distribution given by Eq. (2) must be real,

$$P(\omega_j, \omega_{j'}) = [P(\omega_j, \omega_{j'})]^\star \,. \tag{4}$$

Considering the property of the spherical harmonics

$$C^\star_{kq}(\theta, \phi) = (-1)^q C_{k-q}(\theta, \phi) \,, \tag{5}$$

it can thus be shown that Q must be zero, with

$$[h^K_0(k_1 k_2)]^\star = (-1)^{k_1+k_2+K} h^K_0(k_1 k_2) \,. \tag{6}$$

Specifically, Eq. (2) becomes

$$P(\omega_j, \omega_{j'}) = \frac{1}{16\pi^2} \sum_K \sum_{k_1,k_2} [k_1][k_2]\, h^K_0(k_1 k_2)\, [B^K_0(k_1 k_2; \omega_j, \omega_{j'})]^\star \,, \tag{7}$$

where the relevant bipolar harmonics are[38]

$$[B^K_0(k_1 k_2; \omega_j, \omega_{j'})]^\star = \sum_q \langle k_1 - q, k_2 q | K 0 \rangle \, C_{k_1-q}(\theta_j, 0)\, C^\star_{k_2 q}(\theta_{j'}, \phi_{j'}) \tag{8}$$

2. Symmetry considerations

Next we consider the reflection symmetry properties of the four-vector $\boldsymbol{k}$-$\boldsymbol{k}'$-$\boldsymbol{j}$-$\boldsymbol{j}'$ correlation, as illustrated in Fig. 2. In the $\boldsymbol{k}$-$\boldsymbol{k}'$ scattering frame, the distribution of the product AB internuclear axes is invariant to reflection in the xz plane, containing $\boldsymbol{k}$ and $\boldsymbol{k}'$, provided that the collisional process is achiral. Since both $\boldsymbol{j}$ and $\boldsymbol{j}'$ behave as pseudo vectors, their x and z components change sign under reflection of the nuclear coordinates in the xz plane of the scattering frame[39], whilst the y component is unchanged; *i.e.* $j_x \to -j_x$, $j_y \to j_y$, and $j_z \to -j_z$. Therefore, the effect of the reflection symmetry operation (with operator $\hat{\mathcal{S}}$) on the $\boldsymbol{k}$-$\boldsymbol{k}'$-$\boldsymbol{j}$-$\boldsymbol{j}'$ distribution is (see Fig. 2)

$$\hat{\mathcal{S}}[P(\theta, 0, \theta_j, \varphi_j, \theta_{j'}, \varphi_{j'})] = P(\theta, 0, \pi - \theta_j, \pi - \varphi_j, \pi - \theta_{j'}, \pi - \varphi_{j'}) \,, \tag{9}$$

where φ_j and $\varphi_{j'}$ are the azimuthal angles that define the directions of $\boldsymbol{j}$ and $\boldsymbol{j}'$ with respect to the $\boldsymbol{k}$–$\boldsymbol{k}'$ plane. The vectors $\boldsymbol{k}$ and $\boldsymbol{k}'$ are unaffected by reflection in the scattering plane, whereas the pseudo vectors $\boldsymbol{j}$ and $\boldsymbol{j}'$ change direction, because reflection in a plane changes

the sense of rotation. Given the above mentioned invariance, the distribution on the right hand side of Eq. (9) is the same as the original $P(\theta, 0, \theta_j, \varphi_j, \theta_{j'}, \varphi_{j'})$ distribution.

The $\boldsymbol{k}$-$\boldsymbol{j}$ frame is defined such that the new xz plane contains $\boldsymbol{k}$ and $\boldsymbol{j}$, with the $+x$ direction lying along the direction of $\boldsymbol{j}$. Therefore, in the $\boldsymbol{k}$-$\boldsymbol{j}$ frame, the effect of reflection in the scattering plane on the $\boldsymbol{k}$-$\boldsymbol{k}'$-$\boldsymbol{j}$-$\boldsymbol{j}'$ distribution described in Eq. (9) can be obtained by applying a frame rotation, $\hat{\mathcal{R}}$, of $\pi - \varphi_j$ about the $\boldsymbol{k}$ axis, as shown in Fig. 2,

$$\hat{\mathcal{R}}[P(\theta, 0, \pi - \theta_j, \pi - \varphi_j, \pi - \theta_{j'}, \pi - \varphi_{j'})] = P(\theta, \varphi_j - \pi, \pi - \theta_j, 0, \pi - \theta_{j'}, -\phi_{j'})\,, \tag{10}$$

where $\phi_{j'} = \varphi_{j'} - \varphi_j$, and defines the azimuthal angle of $\boldsymbol{j}'$ in the $\boldsymbol{k}$-$\boldsymbol{j}$ frame. Consequently, the effect of the reflection in the $\boldsymbol{k}$-$\boldsymbol{k}'$ plane on the $\boldsymbol{k}$-$\boldsymbol{k}'$-$\boldsymbol{j}$-$\boldsymbol{j}'$ distribution, as expressed in the $\boldsymbol{k}$-$\boldsymbol{j}$ frame, can be written (with $\phi_j = 0$ taken as implicit)

$$P(\theta, 0, \theta_j, \theta_{j'}, \phi_{j'}) = P(\theta, \varphi_j - \pi, \pi - \theta_j, \pi - \theta_{j'}, -\phi_{j'})\,. \tag{11}$$

Note that this rotation implies defining the $+x$ axis such that the zx plane contains the direction of $\boldsymbol{j}$.

In the case of the three-vector $\boldsymbol{k}$-$\boldsymbol{j}$-$\boldsymbol{j}'$ vector correlation, the distribution of $\boldsymbol{k}'$ is undetermined. Hence, invariance of the three-vector $\boldsymbol{k}$-$\boldsymbol{j}$-$\boldsymbol{j}'$ distribution under reflection in the $\boldsymbol{k}$-$\boldsymbol{j}$ frame reads

$$P(\theta_j, \theta_{j'}, \phi_{j'}) = P(\pi - \theta_j, \pi - \theta_{j'}, -\phi_{j'})\,. \tag{12}$$

Notice that in this case the transformation implies $j_x \to j_x$, $j_y \to -j_y$, and $j_z \to -j_z$.

In order to impose invariance of the distribution under reflection in the scattering plane we can proceed by making use the following properties of the spherical harmonics, which can be derived from the properties of the rotation matrix elements, $d^k_{qq'}(\theta)$[38],

$$C^\star_{kq}(\pi - \theta, -\phi) = (-1)^{k+q} C_{kq}(\theta, \phi) \tag{13}$$

$$C_{kq}(\pi - \theta, 0) = (-1)^{k+q} C_{kq}(\theta, 0)\,. \tag{14}$$

Hence

$$[B^K_0(k_1 k_2; \pi - \theta_j, 0, \pi - \theta_{j'}, -\phi_{j'})]^\star = (-1)^K [B^K_0(k_1 k_2; \theta_j, 0, \theta_{j'}, \phi_{j'})]^\star \tag{15}$$

and

$$h^K_0(k_1 k_2) = (-1)^K h^K_0(k_1 k_2)\,. \tag{16}$$

That is to say, K must be even, and

$$h^K_0(k_1 k_2)^\star = (-1)^{k_1 + k_2} h^K_0(k_1 k_2)\,. \tag{17}$$

3. Expansion coefficients

A more convenient way of dealing with the distributions described above is to expand them in terms of angle dependent moments, the analogues of the polarization dependent differential cross sections (PDDCSs)[7,35,40]:

$$P(\theta_j, \theta_{j'}, \phi_{j'}) = \frac{1}{4\pi} \sum_{k_2} \sum_{q=-k_2}^{q=k_2} [k_2] S_{k_2\, q}(\theta_j) C^{\star}_{k_2 q}(\theta_{j'}, \phi_{j'}) \,, \tag{18}$$

where

$$S_{k_2\, q}(\theta_j) = \langle C_{k_2\, q}(\theta_{j'}, \phi_{j'}) \rangle_{\omega_{j'}} = (-1)^q S^{\star}_{k_2\, -q}(\theta_j) \,, \tag{19}$$

where $\langle ... \rangle_{\omega_{j'}}$ indicates the average over the solid angle subtended by $\theta_{j'}$ and $\phi_{j'}$. By comparison with Eq. (18) and Eq. (7), it is readily shown that the angle dependent moments are given by the expression

$$S_{k_2\, q}(\theta_j) = \frac{1}{2} \sum_{k_1 \geq |q|} [k_1] s^{k_1}_{k_2 q} C_{k_1 - q}(\theta_j, 0) \,, \tag{20}$$

with

$$s^{k_1}_{k_2\, q} = \sum_K \langle k_1 - q, k_2 q | K 0 \rangle \, h^K_0(k_1 k) \,. \tag{21}$$

For calculation purposes, the expression for these coefficients is given by

$$s^{k_1}_{k_2\, q} = \langle C_{k_1 - q}(\theta_j, 0) C_{k_2\, q}(\theta_{j'}, \phi_{j'}) \rangle_{\omega_j, \omega_{j'}} \,, \tag{22}$$

where $\langle ... \rangle_{\omega_j, \omega_{j'}}$ indicates an average over the $P(\theta_j, \theta_{j'}, \phi_{j'})$ distribution.

Note that the symmetry restrictions discussed in Section II A 2 restricts K to even terms in Eq. (21). Furthermore, it also implies

$$s^{k_1}_{k_2\, q} = (-1)^{(k_1 + k_2)} s^{k_1 \star}_{k_2\, q} = (-1)^{(k_1 + k_2)} s^{k_1}_{k_2\, -q} \tag{23}$$

so that when $k_1 + k_2$ is even, the $s^{k_1}_{k_2 q}$ moments are pure real, and when $k_1 + k_2$ is odd, the $s^{k_1}_{k_2 q}$ moments are pure imaginary. This implies that for $q = 0$ only $k_1 + k_2$ even terms contribute to $s^{k_1}_{k_2 0}$. The immediate consequence of Eq. (23) is that Eq. (22) can be written as the expectation values

$$s^{k_1}_{k_2 q} = \langle C_{k_1 q}(\theta_j, 0) C_{k_2 q}(\theta_{j'}, 0) \cos q\phi_{j'} \rangle \qquad k_1 + k_2 \ \text{ even} \tag{24}$$

$$s^{k_1}_{k_2 q} = i \, \langle C_{k_1 q}(\theta_j, 0) C_{k_2 q}(\theta_{j'}, 0) \sin q\phi_{j'} \rangle \qquad k_1 + k_2 \ \text{ odd} \,. \tag{25}$$

By analogy with the $\boldsymbol{k}$-$\boldsymbol{k}'$-$\boldsymbol{j}'$[7,8] and $\boldsymbol{k}$-$\boldsymbol{j}$-$\boldsymbol{k}'$ vector correlations[35], the *conditional* probability density distribution of the direction of $\boldsymbol{j}'$ for a given value of θ_j is given by

$$P(\theta_{j'}, \phi_{j'}|\theta_j) = \frac{P(\theta_j, \theta_{j'}, \phi_{j'})}{P(\theta_j)} = \frac{1}{4\pi} \sum_{k_2,q} [k_2] \, \frac{S_{k_2 q}(\theta_j)}{S_{0\,0}(\theta_j)} \, C^{\star}_{k_2 q}(\theta_{j'}, \phi_{j'}) \, . \tag{26}$$

4. Hertel-Stoll normalization

We now consider the equations appropriate within the Hertel-Stoll normalization[41]. We can define real PDDCSs according to

$$S_{k_2 q+}(\theta_j) = \frac{1}{\sqrt{2}} \left[(-1)^q S_{k_2+q}(\theta_j) + S_{k_2-q}(\theta_j) \right] \tag{27}$$

$$S_{k_2 q-}(\theta_j) = \frac{1}{i\sqrt{2}} \left[(-1)^q S_{k_2+q}(\theta_j) - S_{k_2-q}(\theta_j) \right] \, , \tag{28}$$

with $q \geq 0$. It can be readily shown that the real $S_{kq\pm}(\theta_j)$ polarization moments can be written as

$$S_{k_2 q+}(\theta_j) = \frac{1}{2\sqrt{2}} \sum_{k_1} [k_1] C_{k_1 q}(\theta_j, 0) s^{k_1}_{k_2 q} \left[1 + (-1)^{k_1+k_2} \right] \tag{29}$$

$$S_{k_2 q-}(\theta_j) = \frac{1}{2i\sqrt{2}} \sum_{k_1} [k_1] C_{k_1 q}(\theta_j, 0) s^{k_1}_{k_2 q} \left[1 - (-1)^{k_1+k_2} \right] \, , \tag{30}$$

where use has been made of the relationship given in Eq. (23). Furthermore, with these real PDDCSs, Eq. (18) can be written

$$\begin{aligned} P(\theta_j, \theta_{j'}, \phi_{j'}) = \frac{1}{4\pi} \sum_{k_2} [k_2] \Bigg[& S_{k_2 0}(\theta_j) C_{k_2 0}(\theta_{j'}, 0) \\ & + \sqrt{2} \sum_{q>0} C_{k_2-q}(\theta_{j'}, 0) \Big\{ S_{k_2 q+}(\theta_j) \cos q\phi_{j'} + S_{k_2 q-}(\theta_j) \sin q\phi_{j'} \Big\} \Bigg] \, . \end{aligned} \tag{31}$$

5. k-j correlation.

Integration of Eq. (18) over $(\theta_{j'}, \phi_{j'})$ yields the $\boldsymbol{k}$-$\boldsymbol{j}$ correlation. The orthonormality of the spherical harmonics means that the equation reduces to a single term, $S_{0\,0}(\theta_j)$, with $k_2 = q = 0$. Using Eq. (20), the corresponding $\boldsymbol{k}$-$\boldsymbol{j}$-$\boldsymbol{j}'$ PDDCS with $k_2 = q = 0$ is given by

$$S_{0\,0}(\theta_j) \equiv P(\theta_j) = \frac{1}{2} \sum_{k_1=0} [k_1] s^{k_1}_{0\,0} P_{k_1}(\cos\theta_j) \, . \tag{32}$$

This represents the ***k-j*** *'intrinsic'* distribution[35,37]; that is the (normalized) collision probability for an angle θ_j between $\boldsymbol{k}$ and $\boldsymbol{j}$. Notice that this distribution should not be confused with the 'experimental' or 'extrinsic' preparation of the rotational angular momentum, which is discussed in Section III. The coefficients of the expansion in Eq. (32) are the moments

$$s^{k_1}_{0\,0} = \int_{-1}^{1} P_{k_1}(\cos\theta_j) P(\theta_j)\, \mathrm{d}\cos\theta_{\mathrm{j}} = \langle P_{k_1}(\cos\theta_j)\rangle_{\omega_j}\,. \tag{33}$$

Taking into account Eq. (23), only the $s^{k_1}_{0\,0}$ moments with k_1 even are non-zero.

6. k-j′ correlation.

The ***k-j′*** distribution in the ***k-j*** frame defined above is obtained by integrating equation (7) or equivalently equation (18) over the coordinates of $\boldsymbol{j}$, namely θ_j. The result can be written

$$P(\theta_{j'},\phi_{j'}) = \frac{1}{4\pi}\sum_{k_2 q}[k_2]\, a^{k_2}_q\, C^{\star}_{k_2 q}(\theta_{j'},\phi_{j'})\,, \tag{34}$$

where the $a^{k_2}_q$ polarization parameters can be written

$$a^{k_2}_q = \langle C_{k_2 q}(\theta_{j'},\phi_{j'})\rangle_{\omega_j,\omega_{j'}} = \int_{-1}^{1} S_{k_2 q}(\theta_j)\,\mathrm{d}\cos\theta_j = \frac{1}{2}\sum_{k_1\geq|q|}[k_1] s^{k_1}_{k_2 q}\int_{-1}^{1} C_{k_1 -q}(\theta_j,0)\,\mathrm{d}\cos\theta_j\,. \tag{35}$$

For $q=0$ the integral of the right hand side of this equation is $2\cdot\delta_{k_1,0}$. Hence

$$a^{k_2}_0 = s^0_{k_2 0} = h^{k_2}_0(0 k_2)\,. \tag{36}$$

For the distribution to be real and planar symmetric, the $q=0$ moments with odd values of k_2 must be zero.

To determine the effects of planar symmetry for the $q\neq 0$ moments, it is again better to work within the Hertel-Stoll normalization. Explicitly we have

$$P(\theta_{j'},\phi_{j'}) = \frac{1}{4\pi}\sum_{k_2}[k_2]\left\{a^{k_2}_0 P_{k_2}(\cos\theta_{j'}) + \sqrt{2}\sum_{q>0} C_{k-q}(\theta_{j'},0)[a^{k_2}_{q+}\cos q\phi_{j'} + a^{k_2}_{q-}\sin q\phi_{j'}]\right\}\,,$$

where

$$a^{k_2}_{q+} = \frac{1}{2\sqrt{2}}\sum_{k_1}[k_1] s^{k_1}_{k_2 q}\left[1+(-1)^{k_1+k_2}\right]\int_{-1}^{1} C_{k_1 q}(\theta_j,0)\,\mathrm{d}\cos\theta_j \tag{37}$$

$$a^{k_2}_{q-} = \frac{1}{2i\sqrt{2}}\sum_{k_1}[k_1] s^{k_1}_{k_2 q}\left[1-(-1)^{k_1+k_2}\right]\int_{-1}^{1} C_{k_1 q}(\theta_j,0)\,\mathrm{d}\cos\theta_j\,. \tag{38}$$

Because the integrals over $C_{k_1 q}(\theta_j, 0)$ are only non-zero for even values of $k_1 + q$, this implies that the $a^{k_2}_{q+}$ moments within the Hertel-Stoll normalization are only non-zero for even values of $k_2 + q$, while the $a^{k_2}_{q-}$ moments are non-zero only for moments with odd values of $k_2 + q$.

Finally, the expansion coefficients, $a^k_{q\pm}$, can be written as the following expectation values

$$a^{k_2}_{q+} = (-1)^q \sqrt{2} \langle C_{k_2|q|}(\theta_{j'}, 0) \cos q\phi_{j'} \rangle \qquad k + q \quad \text{even} \tag{39}$$

$$a^{k_2}_{q-} = (-1)^q \sqrt{2} \langle C_{k_2|q|}(\theta_{j'}, 0) \sin q\phi_{j'} \rangle \qquad k + q \quad \text{odd}\,. \tag{40}$$

In the case that the ***k*-*j*** plane is undefined, the ***k*-*j′*** distribution may be obtained by integrating over $\phi_{j'}$. Trivially, this yields a Legendre polynomial, $P_k(x)$, expansion in $\cos\theta_{j'}$:

$$P(\theta_{j'}) = \frac{1}{2} \sum_{k_2} [k_2]\, a^{k_2}_0\, P_{k_2}(\cos\theta_{j'})\,, \tag{41}$$

with $a^{k_2}_0 \equiv h^{k_2}_0(0k_2)$, which only contains k_2 even terms.

7. j-j′ vector correlation.

The ***j*-*j′*** distribution may be obtained by contracting the tensorial product implicit in Eq. (3) when $K = 0$, which implies that $k_1 = k_2 = k$. The resulting expansion may be written (using the notation in reference 13)

$$P(\theta_{jj'}) = \frac{1}{2} \sum_{k} [k]\, a^{(k)}(j, j')\, C_{k0}(\theta_{jj'}, 0)\,, \tag{42}$$

where the moments are defined

$$a^{(k)}(j, j') = \langle P_k(\cos\theta_{jj'}) \rangle = (-1)^k\, [k]^{1/2}\, h^0_0(kk)\,, \tag{43}$$

and $\theta_{jj'}$ is the angle describing the rotational tilt of ***j′*** with respect to ***j***. Note that the depolarization cross sections, determined experimentally in the accompanying paper[34], can be related to the depolarization moments *via* the equation[14,26]

$$\sigma^{(k)}_{jj'} = \sigma_{jj'} \left[1 - a^{(k)}(j, j')\right]\,, \tag{44}$$

where $\sigma_{jj'} \equiv \sigma^{(0)}_{jj'}$ is the integral RET cross section for the collisionally induced transition $j \to j'$. The k odd and k even depolarization cross sections are often referred to as collisional 'disorientation' and 'disalignment' moments, respectively.

8. a-j-j′ correlation

In some of what follows we use the kinematic apse frame rather than a frame in which $\boldsymbol{k}$ is taken as the z-axis. The kinematic apse was defined in Eq. (1)[30], and the apse frame is chosen such that the z-axis coincides with $\boldsymbol{a}$, and the zx-plane contains $\boldsymbol{j}$ (see Fig. 1c). Note that the kinematic apse, $\boldsymbol{a}$, lies in the $\boldsymbol{k}$-$\boldsymbol{k}'$ scattering plane, as shown in Fig. 1a. In the apse frame we use the notation $(\omega_{aj}, \omega_{aj'})$ to identify the coordinates of $\boldsymbol{j}$ and $\boldsymbol{j}'$. The equations of the previous subsection are equally valid in the apse frame, since the two frames are simply related by a rotation about an axis normal to the scattering plane. As noted in the introduction, for an impulsive collision, there can only be a change of rotational angular momentum imparted perpendicular to the scattering plane. This leads to the propensity rule for the conservation of the projection of $\boldsymbol{j}$ along the kinematic apse.

III. LAB FRAME DISTRIBUTION

A. Transformation to the LAB frame

Here we consider the situation in which a molecule is initially aligned or oriented in the laboratory (LAB) by absorption of polarized light. In the case of linearly polarized excitation, the LAB frame is defined such that the Z-axis lies along the direction of the electric vector of the light, and the direction of propagation lies along the X-axis. (Note that the laboratory frame is defined differently if circularly polarized light is used.) In the LAB frame, the distribution of relative velocities, $\boldsymbol{k}$, may be characterized by an expansion

$$P(\Theta_k, \Phi_k) = \frac{1}{4\pi} \sum_{k'q'} [k']\, g^{k'}_{q'}\, C_{k'q'}(\Theta_k, \Phi_k) = \frac{1}{8\pi^2} \sum_{k'q'} [k']\, g^{k'}_{q'}\, D^{k'}_{q'0}{}^{\star}(\Phi_k, \Theta_k, \chi_k)\,, \qquad (45)$$

where Θ_k and Φ_k are the angles that define the direction of $\boldsymbol{k}$ in the LAB frame, and the third Euler angle, χ_k, is arbitrarily defined. The joint distribution of $\boldsymbol{j}$ and $\boldsymbol{j}'$ in the LAB frame can then be obtained by rotation of the bipolar harmonics into the lab frame and

integrating over all orientations of $\boldsymbol{k}$:

$$\begin{aligned} P(\Omega_j, \Omega_{j'}) &= \int P(\Theta_k, \Phi_k) P(\omega_j, \omega_{j'}) \mathrm{d}\Omega_k \\ &= \frac{1}{16\pi^2} \sum_K \sum_{k_1 k_2} [k_1][k_2]\, h_0^K(k_1 k_2) \\ &\times \int P(\Theta_k, \Phi_k) \sum_P D_{P0}^K(\Phi_k, \Theta_k, \chi_k) \left[B_P^K(k_1 k_2; \Omega_j, \Omega_{j'})\right]^\star \mathrm{d}\Omega_k \,. \end{aligned} \tag{46}$$

The orthogonality of the rotation matrices leads to

$$P(\Omega_j, \Omega_{j'}) = \frac{1}{16\pi^2} \sum_K \sum_{k_1 k_2} [k_1][k_2]\, h_0^K(k_1 k_2) \sum_{q'} g_{q'}^K \left[B_{q'}^K(k_1 k_2; \Omega_j, \Omega_{j'})\right]^\star \,. \tag{47}$$

For most cases, q' will be zero because $\boldsymbol{k}$ will be cylindrically distributed about the LAB Z-axis. Furthermore, if $\boldsymbol{k}$ is isotropic, then the only term in the above expansion will be that with $K = q' = 0$, specifically

$$P(\Omega_j, \Omega_{j'}) = \frac{1}{16\pi^2} \sum_k [k]^2\, h_0^0(kk) \left[B_0^0(kk; \Omega_j, \Omega_{j'})\right]^\star \,, \tag{48}$$

which again reduces to a Legendre polynomial expansion in $\Theta_{jj'} \equiv \theta_{jj'}$.

To complete the transformation into the LAB frame, Eqs. (47) and (48) need to be convoluted with the laboratory frame distribution of $\boldsymbol{j}$, that is to say the *extrinsic* distribution of $\boldsymbol{j}$. The latter can be written[13]

$$P(\Theta_j, \Phi_j) = \frac{1}{4\pi} \sum_{k'' q''} [k'']\, r_{q''}^{k''}(j)\, C_{k'' q''}^\star(\Theta_j, \Phi_j) \,. \tag{49}$$

Making use of the orthogonality of the spherical harmonics in Eq. (47), the resulting expansion can be written

$$\begin{aligned} P(\Omega_{j'}) &= \int P(\Theta_j, \Phi_j)\, P(\Omega_j, \Omega_{j'})\, \mathrm{d}\Omega_j \\ &= \frac{1}{4\pi} \sum_K \sum_{k'' k_2} [k''][k_2]\, h_0^K(k'' k_2) \\ &\times \sum_{q' q''} g_{q'}^K\, (-1)^{K-q'-q''} [K]^{1/2} \begin{pmatrix} k'' & K & k_2 \\ -q'' & -q' & q_2 \end{pmatrix} r_{q''}^{k''}(j)\, C_{k_2 q_2}^\star(\Theta_{j'}, \Phi_{j'}) \,. \end{aligned} \tag{50}$$

B. Link with QM expressions

To make contact with the QM expressions[1,13,42,43] it is helpful to use Eq. (50) to obtain the moments of the distribution of $\boldsymbol{j}'$.

$$\mathcal{P}_q^k(j') = \langle C_{kq}(\Theta_{j'}, \Phi_{j'})\rangle = \int P(\Omega_{j'})\, C_{kq}(\Theta_{j'}, \Phi_{j'})\, \mathrm{d}\Omega_{j'}\,. \tag{51}$$

Using the orthogonality of the spherical harmonics these can be written

$$\begin{aligned}\mathcal{P}_q^k(j') &= \langle C_{kq}(\Theta_{j'}, \Phi_{j'})\rangle \\ &= \sum_{Kk''}[k'']\, h_0^K(k''k) \sum_{q'q''} g_{q'}^K\, (-1)^{K+q}[K]^{1/2} \begin{pmatrix} k'' & K & k \\ -q'' & -q' & q \end{pmatrix} r_{q''}^{k''}(j)\,. \end{aligned} \tag{52}$$

That is to say

$$\mathcal{P}_q^k(j') = \sum_{k''q''} a_{qq''}^{kk''}(j,j')\, r_{q''}^{k''}(j)\,, \tag{53}$$

with

$$a_{qq''}^{kk''}(j,j') = [k'']\sum_K \sum_{q'} g_{q'}^K\, (-1)^{K+q}[K]^{1/2} \begin{pmatrix} k'' & K & k \\ -q'' & -q' & q \end{pmatrix} h_0^K(k''k)\,. \tag{54}$$

Note that in the case that the initial distribution of $\boldsymbol{k}$ is isotropic, then $K = 0$, and

$$a_{qq''}^{kk''}(j,j') \equiv a_{qq}^{kk}(j,j') = (-1)^k [k]^{1/2}\, h_0^0(kk)\, \delta_{kk''}\delta_{qq''}\,, \tag{55}$$

in agreement with Eq. (43), and with what one would expect from simpler treatments[13]. Eq. (53) is also consistent with the QM expressions obtained in the previous work of Alexander[43] and of Follmeg *et al.*[42].

Another interesting example is when the direction of $\boldsymbol{k}$ is well defined, and is taken to be along the LAB Z-axis. This is precisely the situation described in references 1 and 43 on the QM $\boldsymbol{k}$-$\boldsymbol{j}$-$\boldsymbol{j}'$ distribution. In this case $(\Phi_k, \Theta_k, \chi_k) = (-\Phi_j, 0, 0)$, and

$$P(\Omega_j, \Omega_{j'}) = \frac{1}{16\pi^2}\sum_K \sum_{k_1k_2}[k_1][k_2]\, h_0^K(k_1k_2) \sum_P D_{P0}^K(-\Phi_j, 0, 0)\left[B_P^K(k_1k_2; \Omega_j, \Omega_{j'})\right]^\star\,. \tag{56}$$

The rotation matrix element $D_{P0}^K(-\Phi_j, 0, 0) = \delta_{P0}$, and therefore in this case the moments of the products can be related to those of the reactants *via* the equation

$$\mathcal{P}_q^k(j') = \sum_{k''} a_{qq}^{kk''}(j,j')\, r_q^{k''}(j)\,, \tag{57}$$

with

$$a_{qq}^{kk''}(j,j') = (-1)^q[k''] \sum_K (-1)^K [K]^{1/2} \begin{pmatrix} k'' & K & k \\ -q & 0 & q \end{pmatrix} h_0^K(k''k) \equiv (-1)^q \, [k''] \, s_{kq}^{k''} \, . \qquad (58)$$

That is to say, the collision can change the rank k but not 'projection' q. The $s_{kq}^{k''}$ moments are the analogues of the quantum mechanical 'correlation' coefficients, which in turn are proportional to the tensor cross sections of Follmeg *et al.*[42].

IV. QCT AND QM CALCULATIONS

A. Classical tensor opacity functions and open shell calculations.

In previous work[13] it has been shown that open shell cross sections for inelastic scattering of molecules in $^2\Sigma^+$ electronic states can also be obtained using QCT calculations, on the assumption that electron and nuclear spin behave as spectators to the dynamics. In this section, the most important equations to achieve this will be presented, and the reader is referred to ref. 13 for further details. Note that the results of these approximate 'open-shell' QCT calculations have been shown previously to be in excellent accord with those from exact QM dynamical calculations for the types of system under discussion[13,14,17].

As previously[12–14,17], we employ the following notation. $\boldsymbol{N}$ ($\boldsymbol{N}'$) denotes the diatomic rotational angular momentum apart from electron and nuclear spin. For a diatomic radical in a $^2\Sigma^+$ electronic state, for which electronic orbital angular momentum is zero, $\boldsymbol{N}$ ($\boldsymbol{N}'$) is equivalent to the nuclear rotational angular momentum, which must lie perpendicular to the internuclear axis, $\boldsymbol{r}$. The corresponding quantum number is written N (N'). The total rotational angular momentum apart from nuclear spin is denoted by $\boldsymbol{j}$, and its quantum number as j. In the Hund's case (b) coupling scheme appropriate for $^2\Sigma^+$ radicals, the molecular wave function is defined by $\boldsymbol{j} = \boldsymbol{N} + \boldsymbol{S}$, where $\boldsymbol{S}$ is the electronic spin. The total angular momentum quantum number of the collision system (*i.e.* NO(A) with He in the application discussed in Section V) is denoted by J and its projection onto the space fixed Z-axis by M_J. Finally, the symbols ℓ and ℓ' refer to the initial and final orbital angular momentum quantum numbers for the collision system.

It is convenient to define the momentum transfer vector as $\boldsymbol{K} = \boldsymbol{N'} - \boldsymbol{N}$, with its

modulus determined by

$$|\boldsymbol{K}|^2 = |\boldsymbol{N}|^2 + |\boldsymbol{N}'|^2 - 2|\boldsymbol{N}||\boldsymbol{N}'|\cos\theta_{NN'}, \tag{59}$$

where

$$\cos\theta_{NN'} = \frac{\boldsymbol{N}\cdot\boldsymbol{N}'}{|\boldsymbol{N}||\boldsymbol{N}'|}\,, \tag{60}$$

and $\theta_{NN'}$ is the asymptotic angle between the initial $\boldsymbol{N}$ and final $\boldsymbol{N}'$ angular momentum vectors.

The moduli of $\boldsymbol{N}$ and $\boldsymbol{N}'$ can be written in terms of the semiclassical quantization rule

$$|\boldsymbol{N}|^2 = N(N+1)\hbar^2 \tag{61}$$

$$|\boldsymbol{N}'|^2 = N'(N'+1)\hbar^2\,. \tag{62}$$

Analogously, the momentum transfer quantum number can be defined as

$$|\boldsymbol{K}|^2 = K(K+1)\hbar^2\,. \tag{63}$$

(The use of the quantization rule $|\boldsymbol{N}|^2 = (N+1/2)^2\hbar^2$, and similarly for $\boldsymbol{N}'$ and $\boldsymbol{K}$, leads to almost identical results except for N=0.)

According to Eq. (59), for definite values of $\boldsymbol{N}$ and $\boldsymbol{N}'$ there is a one to one correspondence between $\boldsymbol{K}$, and hence K, and $\cos\theta_{NN'}$, and therefore the probability density function of $\cos\theta_{NN'}$ as given by Eq. (42) can be related to that for a continuous K as

$$P(K) \approx P(\cos\theta_{NN'})\frac{2[K]}{[N][N']}\,, \tag{64}$$

where the last term is just the Jacobian of the transformation. If the continuous values of K are approximated to their nearest integers, the discrete probability distribution of a given K for given values of N and N' is

$$P(K) = \frac{\mathcal{N}_{NN'}(K)}{\mathcal{N}_{NN'}} \qquad \text{with } \sum_{K=0} P(K) = 1\,, \tag{65}$$

where $\mathcal{N}_{NN'}$ is the number of trajectories from the initial N to the final N' state, and $\mathcal{N}_{NN'}(K)$ the number of those with a momentum transfer K.

It can be shown[13] that the tensor opacity function can be written as

$$P^K(N,N') = (\ell_{\max}+1)^2[N]P(K)\frac{\mathcal{N}_{NN'}}{\mathcal{N}_N}\,, \tag{66}$$

where $\mathcal{N}_N$ is the total number of trajectories (elastic plus inelastic) starting in an initial quantum number N. Given that the expression for the inelastic cross section is

$$\sigma_{NN'} = \pi b_{\max}^2 \frac{\mathcal{N}_{NN'}}{\mathcal{N}_N}\,, \tag{67}$$

and considering that the relation between impact parameter and the orbital angular momentum quantum number, $k_i^2 b_{\max}^2 \approx (\ell_{\max}+1)^2$, where k_i is the initial wave vector, it follows that

$$P^K(N,N') = \frac{k_i^2}{\pi}[N]\sigma_{NN'}P(K) = \frac{k_i^2}{\pi}[N]\sigma_{NN'}(K)\,. \tag{68}$$

Therefore

$$\sigma_{NN'}(K) = \frac{\pi}{k_i^2}(\ell_{\max}+1)^2\frac{\mathcal{N}_{NN'}(K)}{\mathcal{N}_N} = \frac{\pi}{k_i^2}\frac{P^K(N,N')}{[N]}\,, \tag{69}$$

and

$$\sigma_{NN'} = \frac{\pi}{k_i^2}\sum_{K=0}\frac{P^K(N,N')}{[N]}\,. \tag{70}$$

Let us consider first the collisions of a closed shell species ($S=0$), for which $N=j$ and $N'=j'$. The expression for the depolarization cross sections, Eq. (44), can be written[13,14]

$$\sigma_{NN'}^{(k)} = \sigma_{NN'}[1-a^{(k)}(N,N')]\,, \tag{71}$$

with the classical depolarization moments

$$a^{(k)}(N,N') = \langle P_k(\cos\theta_{NN'})\rangle = \frac{1}{\mathcal{N}_{NN'}}\sum_{i=1}^{\mathcal{N}_{NN'}} P_k(\cos\theta_{NN'}^{(i)})\,, \tag{72}$$

where the sum runs over the ensemble of trajectories ending in a given N' rotational state.

The QM expression for the depolarization cross section can be written[13]

$$\sigma_{NN'}^{(k)} = \sum_{K>0}\sigma_{NN'}(K)\left(1-(-1)^{k-K-N-N'}[N]^{\frac{1}{2}}[N']^{\frac{1}{2}}\left\{\begin{array}{ccc} N & N & k \\ N' & N' & K\end{array}\right\}\right)\,, \tag{73}$$

where $\{...\}$ represents a 6-j symbol. Note that summation over $K=0$ is irrelevant since this term contributes to pure elastic scattering wherein not only $\Delta N = 0$ but also $K=0$, *i.e.* the vector $\boldsymbol{N}$ does not change. Using the Racah formula, valid when $N, N', K \gg k$, it can be shown[44,45] that in the asymptotic limit

$$\left\{\begin{array}{ccc} N & N & k \\ N' & N' & K\end{array}\right\} = \left\{\begin{array}{ccc} N & N' & K \\ N' & N & k\end{array}\right\} \sim \frac{(-1)^{k+K+N+N'}}{[N]^{1/2}[N']^{1/2}}\,P_k(\cos\theta_{NN'})\,, \tag{74}$$

where $\cos\theta_{NN'}$ is given by Eq. (60) using the quantization rules Eq. (61)–(63). Substituting Eq. (74) into Eq. (73)

$$\sigma^{(k)}_{NN'} = \sum_{K>0} \sigma_{NN'}(K)\left[1 - P_k(\cos\theta_{NN'})\right] , \tag{75}$$

and making use of Eq. (69) in Eq. (75)

$$\sigma^{(k)}_{NN'} = \frac{\pi}{k_i^2}(\ell_{\max}+1)^2 \sum_{K>0} \frac{\mathcal{N}_{NN'}(K)}{\mathcal{N}_N}\left[1 - P_k(\cos\theta_{NN'})\right] = \sigma_{NN'}\left[1 - \frac{1}{\mathcal{N}_{NN'}}\sum_{K>0}\mathcal{N}_{NN'}(K)P_k(\cos\theta_{NN'})\right] . \tag{76}$$

Considering the one to one correspondence between K and $\cos\theta_{NN'}$, and discretizing their respective values, leads to the following equation

$$\sigma^{(k)}_{NN'} = \sigma_{NN'}\left[1 - \langle P_k(\cos\theta_{NN'})\rangle\right] , \tag{77}$$

thereby recovering Eq. (71).

To determine the polarization parameters in the case of collisions of open shell species in $^2\Sigma$ electronic states, one can use the quasiclassical expression of the $\sigma_{NN'}(K)$ or $P^K(N,N')$, and introduce them in the QM expression in terms of these magnitudes

$$a^{(k)}(j,j') = (-1)^{k-j-j'}\,[j]^{\frac{1}{2}}\,[j']^{\frac{1}{2}}\,\frac{\displaystyle\sum_K (-1)^{-K}\begin{Bmatrix} j & j & k \\ j' & j' & K\end{Bmatrix}\begin{Bmatrix} N & N' & K \\ j' & j & S\end{Bmatrix}^2 \sigma_{NN'}(K)}{\displaystyle\sum_K \begin{Bmatrix} N & N' & K \\ j' & j & S\end{Bmatrix}^2 \sigma_{NN'}(K)} , \tag{78}$$

and the state–to–state cross section

$$\sigma_{N\,j\to N'\,j'} = [j'][N]\sum_K \begin{Bmatrix} N & N' & K \\ j' & j & S\end{Bmatrix}^2 \sigma_{NN'}(K) . \tag{79}$$

Notice that under the assumption of the electronic (and/or nuclear) spin being a spectator, the direction of $\boldsymbol{j}$ can be adequately sampled with a modulus of quantum number $j = N \pm 1/2$, and assuming a fixed direction of $\boldsymbol{S}$ through the collision, the direction of the final angular momentum $\boldsymbol{j'}$ can be analyzed subject to $j' = N' \pm 1/2$. With this implementation, the values of $\sigma_{N\,j\to N'\,j'}$ and $a^{(k)}(j,j')$ can be determined using the equivalent to Eqs. (67) and (72).

B. QCT computational details

To illustrate the above QCT machinery, batches of approximately 1×10^5 trajectories were run for several initial N states at a fixed collision energy of 0.039 eV for NO(A) + He, which corresponds to the mean thermal collision energy at 300 K. The method employed was similar to that described in ref.[46], and will only be described briefly here. The calculations were performed using the NO(A)+He *ab initio* potential energy surface (PES) of Kłos *et al.*[33]. Since the PES has only been calculated using the fixed equilibrium bond length of the radical, the method of Lagrange multipliers was used to force rigid rotor behaviour during the integration of the classical equations of motion. To assign the final state for each trajectory, the square of the rotational angular momentum $|\boldsymbol{N}'|^2 = N'(N'+1)\hbar^2$ was first calculated, and then the values of N' thereby obtained were rounded to the nearest integer.

Trajectories in a state with $N' = N \pm 0.5$ were considered elastic. Elastic collisions, which only change the direction of the velocity, can still lead to depolarization. The criteria for collisional depolarization by elastic collisions is that there should be a minimum angular momentum transfer $K \geq 0.5$[13]. At a fixed collision energy, the inelastic cross sections, $\sigma_{NN'}$, were calculated using Eq. (67). The maximum impact parameter leading to inelastic trajectories was determined by monitoring the change in the rotational quantum number, ΔN, with the criterion that no trajectories with $|\Delta N| > 0.5$ took place for $b > b_{\max}$. Eq. (67) implies that the impact parameter for the i-th trajectory is sampled according to $b^{(i)} = \xi^{1/2} b_{\max}$, where ξ is a random number in the $(0, 1)$ interval. The QCT calculation of the $a^{(k)}(N, N')$ polarization parameters consisted simply of determining $\cos\theta_{NN'}$ for each trajectory[13], and then applying Eq. (72). Depolarization cross sections were determined from the depolarization parameters and the RET cross sections using Eq. (44).

The above treatment is appropriate for QCT calculations in which NO(A) + He is treated as a closed shell system. QCT estimates of the 'open shell' spin-rotation level changing cross sections for NO(A) + He are also presented here, and were obtained using the procedures discussed in Section IV A and ref.[13].

C. QM computational details

For comparison with some of the QCT results, fully quantum close-coupling (CC) scattering calculations were also performed using the same NO(A)+He *ab initio* PES of Kłos *et al.*[33] used in the QCT calculations. As in our previous work[12–14], the open shell (o–s) electronic structure of the NO(A) molecule was taken into account in the QM scattering calculations using the HIBRIDON suite of codes[47], which employs a hybrid propagator comprised of the Log-Derivative propagator by Manolopoulos[48,49] and the Airy propagator for the long-range region.

In the CC scattering calculations of the closed shell NO(A) + He system, the rotational basis of NO(A) was set to a maximum value of $N = 16$ for the total energy of $326\,\mathrm{cm}^{-1}$ which corresponds to a collision energy of $0.039\,\mathrm{eV}$ for N=2. It was necessary to include partial waves up to $J = 100$. The o–s CC QM scattering calculations were performed with similar convergence and basis parameters as in the case of the c–s calculations.

In the following, we also make a direct comparison between the QCT and QM tensor opacities. The QM tensor opacities of an open shell Hund's case (b) molecules are defined in terms of the reduced matrix elements of the $\boldsymbol{T}$ operator by[13,43,50–52]

$$P^K(N, N') = \frac{1}{[K]} \sum_{\ell\,\ell'} |\langle N'\ell' || T^K || N\ell \rangle|^2 \,, \tag{80}$$

where the reduced $\boldsymbol{T}$-matrix elements have been presented previously in references 43, 51 and 52. Note that the latter are the dynamical quantities obtained from a closed shell scattering calculation[43,50–52]. They have no dependence on the electron spin, and can therefore be calculated from a closed shell calculation. Both closed and open shell integral integral cross-sections calculated using the QM tensor opacities, employing Eqs. (69) and (79), were in excellent agreement with those obtained directly from HIBRIDON.

V. CALCULATION RESULTS AND DISCUSSION FOR NO(A) + He

In the following we illustrate the theoretical methodology presented in Sections II and III by applying it to the RET and angular momentum depolarization collisions of NO(A) + He. As already noted, inelastic scattering and collisional depolarization in this system has been the subject of a previous experimental and theoretical investigation[17], where it was shown

that the results of the 'open shell' calculations agree very well with the experimental findings. The main focus of the following is to show how analysis of the various vector correlations presented here can be used to provide mechanistic insight about the NO(A) + He system. For clarity, we have focussed on a specific RET transition, $N = 2 \rightarrow N' = 3$, but similar results would have been obtained for other RET processes, particularly those in which collisions increase the rotational excitation. It should also be emphasized that the treatment presented here can be used to calculate elastic depolarization cross sections[13], which is a feature of the methodology illustrated in the accompanying paper[34]. In the following, we show the closed shell results first, with the open shell data presented in Subsection V D.

A. $\boldsymbol{k}$-$\boldsymbol{k}'$-$\boldsymbol{j}'$ vector correlation

We start by presenting the classical $\boldsymbol{k}$-$\boldsymbol{k}'$-$\boldsymbol{j}'$ vector correlation[7], which describes the polarization of the product rotational polarization with respect to the scattering plane. Notice that in this subsection as well as in the next one, $\boldsymbol{N}'$ and $\boldsymbol{j}'$ are interchangeable. The left panels of Fig. 3 show the conditional probability density, $P(\theta_{j'}, \phi_{j'}|\theta)$, at selected angles in the range $\theta = 0^\circ$ to $\theta = 180^\circ$. In this and subsequent figures the z-axis is oriented vertically, and the $+x$-axis points towards the left of the figures. Note that for consistency with the analogous QM results, the number of moments, k_2, used to construct the $\boldsymbol{k}$-$\boldsymbol{k}'$-$\boldsymbol{j}'$ distributions shown in the figure is restricted to $2N'$ (*i.e.* $k_{2\,\mathrm{max}} = 6$ for the transition shown). The $\boldsymbol{k}$-$\boldsymbol{k}'$-$\boldsymbol{j}'$ distributions are generally rather broad, suggesting that $\boldsymbol{j}'$ is distributed over a wide range of angles. When the products are forward scattered (top panel), the distribution is slightly peaked with $\boldsymbol{j}'||\boldsymbol{k}$. However, because of the $\sin\theta$ weighting, note that products scattered near to the forward or backward directions contribute less to the scattering dynamics than those born in sideways directions. A more representative picture of the $\boldsymbol{k}$-$\boldsymbol{k}'$-$\boldsymbol{j}'$ correlation is obtained at scattering angles away from $\theta = 0^\circ$ or 180°, for which $\boldsymbol{j}'$ is much more broadly distributed with respect to the scattering plane.

The left panel of Fig. 4 shows the $\boldsymbol{k}$-$\boldsymbol{k}'$-$\boldsymbol{j}'$ distribution obtained by integrating over the scattering angle, θ, but preserving the scattering plane as coincident with the xz plane (*i.e.* the results of Eq. (34)). Once averaged over scattering angle the resulting distribution provides relatively little information about the scattering dynamics. Although, on average, $\boldsymbol{j}'$ is weakly polarized around angles close to 45° to the z-axis, in the zx-plane, the averaging

of the alignment over scattering angle masks the more structured scattering angle-dependent features shown in Fig. 3.

B. $\boldsymbol{k}$-$\boldsymbol{j}$-$\boldsymbol{j}'$ vector correlation

Rather more informative are the plots of the $\boldsymbol{k}$-$\boldsymbol{j}$-$\boldsymbol{j}'$ vector correlation. The conditional probability density, $P(\theta_{j'}, \phi_{j'}|\theta_j)$, is shown in the middle panels of Fig. 3, again for selected angles in the range $\theta_j = 0°$ to 180°. Note that in the cases of the $\boldsymbol{k}$-$\boldsymbol{j}$-$\boldsymbol{j}'$ and $\boldsymbol{a}$-$\boldsymbol{j}$-$\boldsymbol{j}'$ correlations, for consistency with the corresponding QM results, the number of moments, k_2, used to construct the distributions shown in these figures is restricted to $2N$ or $2N'$, whichever is smaller (*i.e.* $k_{2\,\mathrm{max}} = 4$ for the transition shown). In the $\boldsymbol{k}$-$\boldsymbol{j}$ frame, it is immediately apparent that $\boldsymbol{j}'$ has a strong tendency to be polarized along the initial direction of $\boldsymbol{j}$. Collisions between NO(A) and He are only weakly depolarizing, as discussed further below, and thus the distribution of $\boldsymbol{j}'$ is quite narrowly distributed about $\boldsymbol{j}$. As shown in the middle panel of Fig. 4, once the $\boldsymbol{k}$-$\boldsymbol{j}$-$\boldsymbol{j}'$ distribution is integrated over the direction of $\boldsymbol{j}$ (*i.e.* over θ_j), whilst preserving the $\boldsymbol{kj}$ plane, the resulting $P(\theta_{j'}, \phi_{j'})$ distribution is necessarily less informative than which are those resolved in θ_j shown in Fig. 3. Nevertheless, some modest propensity for $\boldsymbol{j}'$ to lie in the $\boldsymbol{kj}$ plane is preserved, as might be expected if NO(A) + He collisions are only weakly depolarizing. Furthermore, on average, $\boldsymbol{j}'$ is seen to be weakly polarized perpendicular to the initial relative velocity vector, $\boldsymbol{k}$, as one might expect.

C. $\boldsymbol{a}$-$\boldsymbol{j}$-$\boldsymbol{j}'$ vector correlation

The right panels of Fig. 3 show the $\boldsymbol{a}$-$\boldsymbol{j}$-$\boldsymbol{j}'$ vector correlation, again presented in the form of a conditional probability density, $P(\theta_{aj'}, \phi_{aj'}|\theta_{aj})$, for θ_{aj} angles in the range 0° to 180°. The distribution at $\theta_{aj} = 0°$ and 180° is particularly revealing. It provides very convincing evidence for the strong propensity for the conservation of the projection of $\boldsymbol{j}$ along the kinematic apse. Because $j < j'$, this can only be achieved if $\boldsymbol{j}'$ lies at some angle to the apse direction, $\boldsymbol{a}$. As the angle between $\boldsymbol{j}$ and the apse $\boldsymbol{a}$ increases, $\boldsymbol{j}'$ tends to follow the direction of $\boldsymbol{j}$, approximately conserving the projection along the apse direction (the z-axis in these figures). Interestingly, apart from when $\theta_{aj} = 0°$ and 180°, in general $\boldsymbol{j}'$ is not distributed with cylindrical symmetry about the apse direction, not least because collisions

favour small angles, $\theta_{jj'}$, between $\boldsymbol{j}$ and $\boldsymbol{j}'$.

As shown in the right panel of Fig. 4, integrating the $\boldsymbol{a}$-$\boldsymbol{j}$-$\boldsymbol{j}'$ distribution over θ_{aj} (but keeping the $\boldsymbol{aj}$ plane aligned parallel with the zx plane) again unsurprisingly results in a loss of information. However, of the three distributions presented the integrated $\boldsymbol{a}$-$\boldsymbol{j}$-$\boldsymbol{j}'$ distribution shows the strongest polarization, with a clear preference observed for $\boldsymbol{j}'$ to lie along the x axis in the $\boldsymbol{a}$-$\boldsymbol{j}$ frame. This reflects the fact that, on average, $\boldsymbol{j}$ tends to lie at 90° to the apse direction, and, as we have already established for this system, $\boldsymbol{j}'$ has a tendency to lie parallel to $\boldsymbol{j}$.

The data shown in this section so far, in particular those presented in Fig. 3, are consistent with previous work on the collisional depolarization of NO(A) by He[17]. The potential energy surface[33] for NO(A) + He possesses only a very modest energy well of $<1\,\mathrm{cm}^{-1}$, and is largely repulsive in nature. Both elastic and RET collisions of NO(A) + He can thus be described quite reliably in terms of hard shell encounters, for which the projection of $\boldsymbol{j}$ onto the apse is rigorously conserved during collision[31,32]. Kinematic factors, in particular the light mass of He, also favour collisions which lead to little angular momentum depolarization, and hence also conserve the projection of $\boldsymbol{j}$ along the kinematic apse.

D. $\boldsymbol{j}$-$\boldsymbol{j}'$ vector correlation

We conclude this illustration by presenting results for the $\boldsymbol{j}$-$\boldsymbol{j}'$ vector correlation for NO(A) + He. This correlation is of particular interest as it is one of the vector correlations most amenable to experimental interrogation[11–25]. In the upper panel of Fig. 5 we illustrate how the classical $\boldsymbol{j}$-$\boldsymbol{j}'$ two-vector correlation for NO(A) + He undergoing the $N = 2 \rightarrow N' = 3$ transition can be factored into regions corresponding to the amount of angular momentum transferred, K. Similar data have been presented previously for OH(A) + Ar[13]. Use of Eq. (69) allows determination of the K-dependent cross sections, $\sigma_{NN'}(K)$, as shown in the lower panel of Fig. 5. These data can then be used to determine the 'closed shell' and 'open shell' depolarization moments, $a^{(k)}_{NN'}$ and $a^{(k)}_{jj'}$, presented in Fig. 6 for collisionally induced disorientation ($k = 1$ – left panels) and disalignment ($k = 2$ – right panels). The closed shell moments, shown in the upper panels of Fig. 6, generally take large positive values, quite close to unity. This is consistent with Eq. (44), and with the fact that NO(A) + He collisions are only weakly depolarizing, as we have seen from the three-vector correlations

already presented. Note that when the depolarization moments are unity, no collisional depolarization takes place and the depolarization cross sections go to zero. The behaviour of the $N = 2 \rightarrow N' = 0$ transition is notably different from the other transitions presented. The reason for this is that the final state, $N' = 0$, cannot be polarized, and thus every collision which induces a transition from $N = 2$ to $N' = 0$ leads to complete angular momentum depolarization.

The 'open shell' QCT depolarization moments for initial $N = 2$ and $j = N + S = 2.5$ shown in the lower panels of Fig. 6 reveal that spin-rotation (SR) conserving transitions are much less depolarizing than spin-rotation changing collisions. This is a direct consequence of the fact that electron spin is treated as a spectator to the dynamics[13]. Transitions which change spin-rotation state must change the direction of the rotational angular momentum, and thus tend to be more depolarizing than the spin-rotation conserving transitions.

The corresponding closed and open shell rotational energy transfer cross sections, $\sigma_{j\,j'}$, for the same initial state ($N = 2, j = 2.5$) as shown in Fig. 6, are presented in Fig. 7. As in the Fig. 6, the 'open shell' QCT cross section data shown in the lower panel of Fig. 7 are resolved into spin-rotation conserving and changing collisions. It can readily be seen that although spin-rotation changing collisions are highly depolarizing, they have rather small cross sections for this system. The reason for this is now clear. Spin-rotation changing collisions require a change in the direction of $\boldsymbol{N}$, and collisional depolarization is rather inefficient for NO(A) + He.

Figs. 5–7 also include a comparison of the closed and open shell QCT calculations with the corresponding QM data. Generally, the integral cross sections and alignment moments calculated classically are in very good agreement with the corresponding quantum mechanical quantities. The exceptions to this are the cross sections for $\Delta N = 1$, which the QCT calculations tend to overestimate. As already mentioned in Section IV, the origin of this problem is the misassignment of trajectories as inelastic in the QCT calculations, rather than elastic. The K-resolved cross sections, $\sigma_{NN'}(K)$, shown in the lower panel of Fig. 5 serve to highlight this point. Notice that for $K > 1$ the QM and QCT data are in excellent accord, whereas the data for $K = 1$ is overestimated in the QCT calculations. If the criteria for binning the $K = 1$ trajectories is changed from a minimum momentum transfer of $K_{\rm min} = 0.5$ to $K_{\rm min} = 1.0$, then the $K = 1$ cross section, $\sigma_{NN'}(K)$, is brought into much better agreement with QM theory. Interestingly, a similar change in $K_{\rm min}$ has only a very

minor effect on the QCT polar plots of the three-vector distributions shown in Figs. 3 and 4. This is also reflected in the QCT polarization parameters shown in Fig. 6, which are generally in better agreement with the QM calculations for the $\Delta N = 1$ transitions than might be expected from the integral cross section data shown in Fig 7.

The excellent agreement between the QCT and QM 'open shell' polarization parameters and integral cross sections is something commented on previously[13]. For $^2\Sigma$ radicals of the type in question, both electron and nuclear spin can be treated reliably as spectators to the dynamics, and the good agreement between QM and QCT theory for these systems primarily reflects the good agreement in the corresponding 'closed shell' tensor opacities. The coupling to the electron and nuclear spin can in fact be treated in the same way in the QM and QCT calculations, since both calculations can be represented in the tensor opacity formalism. A similar approach could be adapted to $^3\Sigma$ linear radicals and to non-linear polyatomic radicals. However, it seems unlikely that a similar approach to that adopted here and elsewhere[13] will be transferable to $^2\Pi$ radicals, or more generally to systems displaying large spin-orbit coupling. In particular, treatment of collisions of $^2\Pi$ radicals within the 'spectator' framework would require allowing for scattering on more than one potential energy surface[53].

VI. CONCLUSIONS

In this paper we have presented the QCT methods required to characterize the angular momentum polarization of the products of inelastic and reactive scattering, paying particular attention to the two- and three- vector correlations involving the initial and final rotational angular momenta, $\boldsymbol{j}$ and $\boldsymbol{j}'$. We have presented the theory that enables the calculation of vector properties which can be directly compared with experimental measurement. The classical theory has been applied to collisional depolarization and RET in the NO(A) + He system, and the results are used to illustrate the type of mechanistic information provided by such calculations. The data support previous conclusions[17] that the projection of $\boldsymbol{j}$ along the kinematic apse is nearly conserved for this system under thermal collision energy conditions. Further applications of the theory developed here are explored in the accompanying paper[34], which presents a comparison of the mechanisms of collisional depolarization and rotational energy transfer for the NO(A) and OH(A) collisions with Ar. In that paper, we further illustrate the mechanistic insight that can be gained by observing two and three-vector

correlations involving the reactant and product angular momenta, $\boldsymbol{j}$ and $\boldsymbol{j}'$.

Acknowledgments

The support of the UK EPSRC (to M.B. *via* Programme Grant No. EP/G00224X/1), the EU (to M.B. *via* FP7 EU People ITN project 238671), and the Spanish Ministry of Science and Innovation (grants CTQ2008-02578/BQU and Consolider Ingenio 2010 CSD2009-00038) are gratefully acknowledged. J.K. acknowledges financial support from the US National Science Foundation (grant No. CHE-0848110 to Professor M.H. Alexander) and the University Complutense de Madrid/Grupo Santander (under the "Movilidad de Investigadores Extranjeros" programme).

REFERENCES

[1]M. P. de Miranda and D. C. Clary, J. Chem. Phys. **106**, 4509 (1997).

[2]D. A. Case and D. R. Herschbach, Mol. Phys. **30**, 1537 (1975).

[3]D. A. Case and D. R. Herschbach, J. Chem. Phys **64**, 4212 (1976).

[4]D. A. Case, G. M. McClelland, and D. R. Herschbach, Mol. Phys. **35**, 541 (1978).

[5]G. M. McClelland and D. R. Herschbach, J. Phys. Chem **83**, 1445 (1979).

[6]J. D. Barnwell, J. G. Loeser, and D. R. Herschbach, J. Phys. Chem **87**, 2781 (1983).

[7]F. J. Aoiz, M. Brouard, and P. A. Enriquez, J. Chem. Phys. **105**, 4964 (1996).

[8]M. P. de Miranda, F. J. Aoiz, L. Bañares, and V. S. Rábanos, J. Chem. Phys **111**, 5368 (1999).

[9]E. A. Wade, K. T. Lorenz, D. W. Chandler, J. W. Barr, G. L. Barnes, and J. I. Cline, Chem. Phys **301**, 261 (2004).

[10]K. T. Lorenz, D. W. Chandler, J. W. Barr, W. Chen, G. L. Barnes, and J. I. Cline, Science **293**, 2063 (2001).

[11]M. Brouard, A. Bryant, I. Burak, F. Quadrini, S. Marinakis, I. A. Garcia, and C. Vallance, Mol. Phys. **103**, 1693 (2005).

[12]J. Kłos, M. H. Alexander, M. Brouard, C. J. Eyles, and F. J. Aoiz, J. Chem. Phys. **129**, 054301 (2008).

[13]F. J. Aoiz, M. Brouard, C. J. Eyles, J. Kłos, and M. P. de Miranda, J. Chem. Phys. **130**, 044305 (2009).

[14]M. Brouard, A. Bryant, Y.-P. Chang, R. Cireasa, C. J. Eyles, A. M. Green, S. Marinakis, F. J. Aoiz, and J. Kłos, J. Chem. Phys. **130**, 044306 (2009).

[15]M. Brouard, H. Chadwick, Y.-P. Chang, R. Cireasa, and C. J. Eyles, Physica Scripta **80**, 048120 (2009).

[16]M. L. Costen, R. Livingstone, K. G. McKendrick, G. Paterson, M. Brouard, H. Chadwick, Y.-P. Chang, C. J. Eyles, F. J. Aoiz, and J. Kłos, J. Phys. Chem. A **113**, 15156 (2009).

[17]M. Brouard, H. Chadwick, Y.-P. Chang, R. Cireasa, C. J. Eyles, A. O. L. Via, N. Screen, F. J. Aoiz, and J. Kłos, J. Chem. Phys. **131**, 104307 (2009).

[18]H. J. Crichton, M. L. Costen, and K. G. McKendrick, J. Chem. Phys. **119**, 9461 (2003).

[19]M. L. Costen, H. J. Crichton, and K. G. McKendrick, J. Chem. Phys. **120**, 7910 (2004).

[20]S. Marinakis, G. Paterson, J. Kłos, M. L. Costen, and K. G. McKendrick, Phys. Chem. Chem. Phys. **9**, 4414 (2007).

[21]S. Marinakis, G. Paterson, G. Richmond, M. Rockingham, M. L. Costen, and K. G. McKendrick, J. Chem. Phys. **128**, 021101 (2008).

[22]G. Paterson, S. Marinakis, M. L. Costen, K. G. McKendrick, J. Kłos, and R. Tobota, J. Chem. Phys. **129**, 074304 (2008).

[23]G. Paterson, S. Marinakis, J. Kłos, M. L. Costen, and K. G. McKendrick, Phys. Chem. Chem. Phys. **11**, 8804 (2009).

[24]G. Paterson, S. Marinakis, M. L. Costen, and K. G. McKendrick, Phys. Chem. Chem. Phys. **11**, 8813 (2009).

[25]I. Ballingall, M. Rutherford, K. McKendrick, and M. Costen, Mol. Phys. **108**, 847 (2010).

[26]P. J. Dagdigian and M. H. Alexander, J. Chem. Phys. **130**, 094303 (2009).

[27]P. J. Dagdigian and M. H. Alexander, J. Chem. Phys. **130**, 164315 (2009).

[28]P. J. Dagdigian and M. H. Alexander, J. Chem. Phys. **130**, 204304 (2009).

[29]L. Ma, M. H. Alexander, and P. J. Dagdigian, J. Chem. Phys. **134**, 154307 (2011).

[30]A. J. McCaffery, M. J. Proctor, and B. J. Whitaker, Annu. Rev. Phys. Chem. **37**, 223 (1986).

[31]V. Khare, D. J. Kouri, and D. K. Hoffman, J. Chem. Phys. **74**, 2275 (1981).

[32]D. K. Hoffman, J. W. Evans, and D. J. Kouri, J. Chem. Phys. **80**, 144 (1984).

[33]J. Kłos, M. H. Alexander, R. Hernández-Lamoneda, and T. G. Wright, J. Chem. Phys.

129, 244303 (2008).

[34]M. Brouard, H. Chadwick, Y.-P. Chang, C. J. Eyles, F. J. Aoiz, and J. Kłos, J. Chem. Phys. (2011).

[35]J. Aldegunde, M. P. de Miranda, J. M. Haigh, B. K. Kendrick, V. Sáez-Rábanos, and F. J. Aoiz, J. Phys. Chem. A **109**, 6200 (2005).

[36]M. P. de Miranda and F. J. Aoiz, Phys. Rev. Lett. **93**, 083201 (2004).

[37]M. P. de Miranda, F. J. Aoiz, M. Brouard, and V. Sáez-Rábanos, J. Chem. Phys. **121**, 9830 (2004).

[38]R. N. Zare, *Angular Momentum, Understanding Spatial Aspects in Chemistry and Physics* (John Wiley and Sons, 1988).

[39]K. Blum, *Density Matrix Theory and Applications, 2nd Ed.* (Plenum Press, New York, 1996).

[40]N. E. Shafer-Ray, A. J. Orr-Ewing, and R. N. Zare, J. Phys. Chem. **99**, 7591 (1995).

[41]I. V. Hertel and W. Stoll, Adv. At. Mol. Phys **13**, 113 (1978).

[42]B. Follmeg, P. Rosmus, and H.-J. Werner, J. Chem. Phys **93**, 4687 (1990).

[43]M. H. Alexander and S. L. Davis, J. Chem. Phys. **78**, 6754 (1983).

[44]A. R. Edmonds, *Angular Momentum in Quantum Mechanics* (Princeton University Press, 1974).

[45]D. A. Varshalovich, A. N. Moskalev, and V. K. Khersonskii, *Quantum Theory of Angular Momentum* (World Scientific, 1988).

[46]F. J. Aoiz, J. E. Verdasco, V. J. Herrero, V. S. Rábanos, and M. H. Alexander, J. Chem. Phys. **119**, 5860 (2003).

[47]HIBRIDON is a package of programs for the time-independent quantum treatment of inelastic collisions and photodissociation written by M. H. Alexander, D. Manolopoulos, H.-J. Werner, and B. Follmeg, with contributions by P. F. Vohralik, D. Lemoine, G. Corey, R. Gordon, B. Johnson, T. Orlikowski, A. Berning, A. Degli-Esposti, C. Rist, P. Dagdigian, B. Pouilly, G. van der Sanden, M. Yang, F. de Weerd, S. Gregurick, and J. Klos.

[48]D. E. Manolopoulos, J. Chem. Phys. **85**, 6425 (1986).

[49]M. H. Alexander and D. E. Manolopoulos, J. Chem. Phys. **86**, 2044 (1987).

[50]G. C. Corey and F. R. McCourt, J. Phys. Chem. **87**, 2723 (1983).

[51]G. C. Corey and A. D. Smith, J. Chem. Phys. **83**, 5663 (1985).

[52]G. C. Corey, M. H. Alexander, and J. Schaefer, J. Chem. Phys. **85**, 2726 (1986).

[53]M. H. Alexander, J. Chem. Phys. **76**, 5974 (1982).

FIG. 1. (Color online.) The reference frames used for considering the three-vector correlations. a) The scattering frame used for the $\boldsymbol{k}$-$\boldsymbol{k}'$-$\boldsymbol{j}'$ correlation, in which $\boldsymbol{k}$ is defined as lying along the z-axis and $\boldsymbol{k}'$ in the zx-plane. b) The frame used to define the $\boldsymbol{k}$-$\boldsymbol{j}$-$\boldsymbol{j}'$ correlation. c) The apse frame used to define the $\boldsymbol{a}$-$\boldsymbol{j}$-$\boldsymbol{j}'$ vector correlation. Note that a simple rotation around the y-axis of the scattering frame results in the kinematic apse, $\boldsymbol{a}$, becoming the z-axis.

FIG. 2. (Color online.) The effect of reflection, $\hat{\mathcal{S}}$, in the scattering $\boldsymbol{k}$-$\boldsymbol{k}'$ plane on the four vector, $\boldsymbol{k}$-$\boldsymbol{k}'$-$\boldsymbol{j}$-$\boldsymbol{j}'$ distribution. The top and centre figures show the effect in the $\boldsymbol{k}$-$\boldsymbol{k}'$ scattering frame and bottom figure shows the result of rotation $\hat{\mathcal{R}}$ into the $\boldsymbol{k}$-$\boldsymbol{j}$ frame. The two frames are connected by a simple rotation about the z-axis, as discussed in the text.

FIG. 3. (Color online.) Left Panels: An illustration of the $\boldsymbol{k}$-$\boldsymbol{k}'$-$\boldsymbol{j}'$ conditional probability density distribution, $P(\theta_{j'}, \phi_{j'}|\theta)$, for NO(A)+ He undergoing the $N = 2 \rightarrow N' = 3$ rotational energy transfer transition at a collision energy of 0.039 eV. The distribution is shown (from top to bottom) at $\theta_{k'} = 0°$, 45°, 90°, 135°, and 180°. Middle panels: As for the left panels but showing the $\boldsymbol{k}$-$\boldsymbol{j}$-$\boldsymbol{j}'$ conditional probability density distribution, $P(\theta_{j'}, \phi_{j'}|\theta_j)$ for a selection of angles, θ_j. Right panels: As for the left panels but showing the $\boldsymbol{a}$-$\boldsymbol{j}$-$\boldsymbol{j}'$ probability density distribution, $P(\theta_{aj'}, \phi_{aj'}|\theta_{aj})$ for a selection of angles, θ_{aj}.

FIG. 4. (Color online.) Left panel: An illustration of the $\boldsymbol{k}$-$\boldsymbol{k}'$-$\boldsymbol{j}'$ probability density distribution, $P(\theta_{j'}, \phi_{j'})$, for NO(A)+ He undergoing the $N = 2 \rightarrow N' = 3$ rotational energy transfer transition at a collision energy of 0.039 eV, integrated over all scattering angles, θ. Note that in this figure, the $\boldsymbol{k}$-$\boldsymbol{k}'$ scattering plane is the zx plane. Middle panel: As for the left panel, but showing the $\boldsymbol{k}$-$\boldsymbol{j}$-$\boldsymbol{j}'$ conditional probability density distribution, $P(\theta_{j'}, \phi_{j'})$. Note that in this figure, the $\boldsymbol{k}$-$\boldsymbol{j}$ plane is the zx plane. Right panel: As for the left panel but showing the $\boldsymbol{a}$-$\boldsymbol{j}$-$\boldsymbol{j}'$ probability density distribution, $P(\theta_{aj'}, \phi_{aj'})$ integrated over all angles θ_{aj}. Note that in this figure, the $\boldsymbol{a}$-$\boldsymbol{j}$ plane is the zx plane.

FIG. 5. (Color online.) Top panel: The $\boldsymbol{j}$-$\boldsymbol{j}'$ distribution showing the partitioning into different amounts of momentum transfer, K. The various momentum transfer 'bins' are identified with dashed (odd K) and continuous (even K) lines in light grey (red online). Bottom panel: The resulting QCT depolarization cross sections, $\sigma_{NN'}(K)$, shown as circles, plotted as a function of momentum transfer, K. The results are compared with the K-resolved cross sections obtained from the QM tensor opacities (triangles). The data are for the $N = 2 \rightarrow N' = 3$ collisionally induced transition for NO(A) + He at a collision energy of 0.039 eV. See text and ref.[13].

FIG. 6. (Color online.) Disorientation (left panels) and disalignment (right panels) moments for NO(A) + He with $N = 2$, resolved in final state at a collision energy of 0.039 eV. The top row shows the QCT (circles) and CC-QM (triangles) closed shell data, whilst the bottom row shows the results of the 'open shell' QCT (circles) and open shell CC-QM (triangles) calculations, with $j = N + S = 2.5$. SR refers to the spin-rotation level, and the figure indicates whether it is conserved, $j' = N' + 1/2$, (labelled cons) or changed, $j' = N' - 1/2$, (change) during collision.

FIG. 7. (Color online.) Upper panel: The closed shell QCT (circles) and CC-QM (triangles) rotational energy transfer cross sections for NO(A) + He at a collision energy of 0.039 eV for initial state $N = 2$. The data are resolved in final rotational state. Lower panel: The QCT 'open shell' and CC-QM open-shell RET cross sections for NO(A) + He with $N = 2$, and $j = N + S = 2.5$, resolved in final state. SR refers to the spin-rotation level, and the figure indicates whether it is conserved, $j' = N' + 1/2$, (labelled cons) or changed, $j' = N' - 1/2$, (change) during collision.

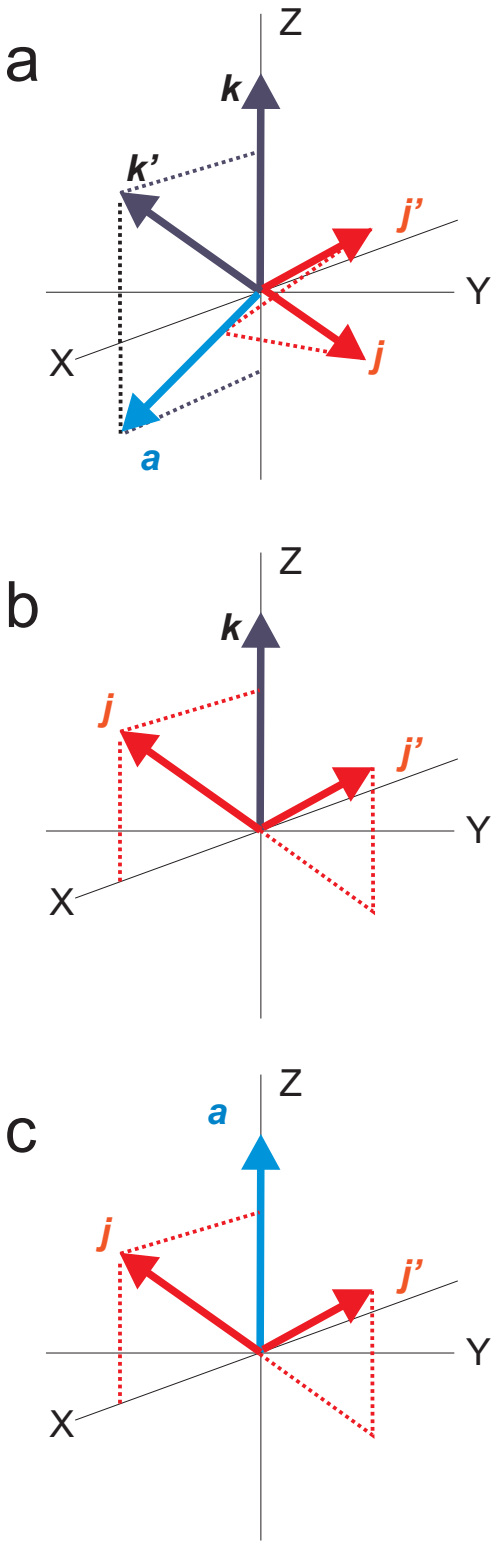
a
Z
k
k'
j'
Y
X
j
a
b
Z
k
j
j'
Y
X
c
Z
a
j
j'
Y
X

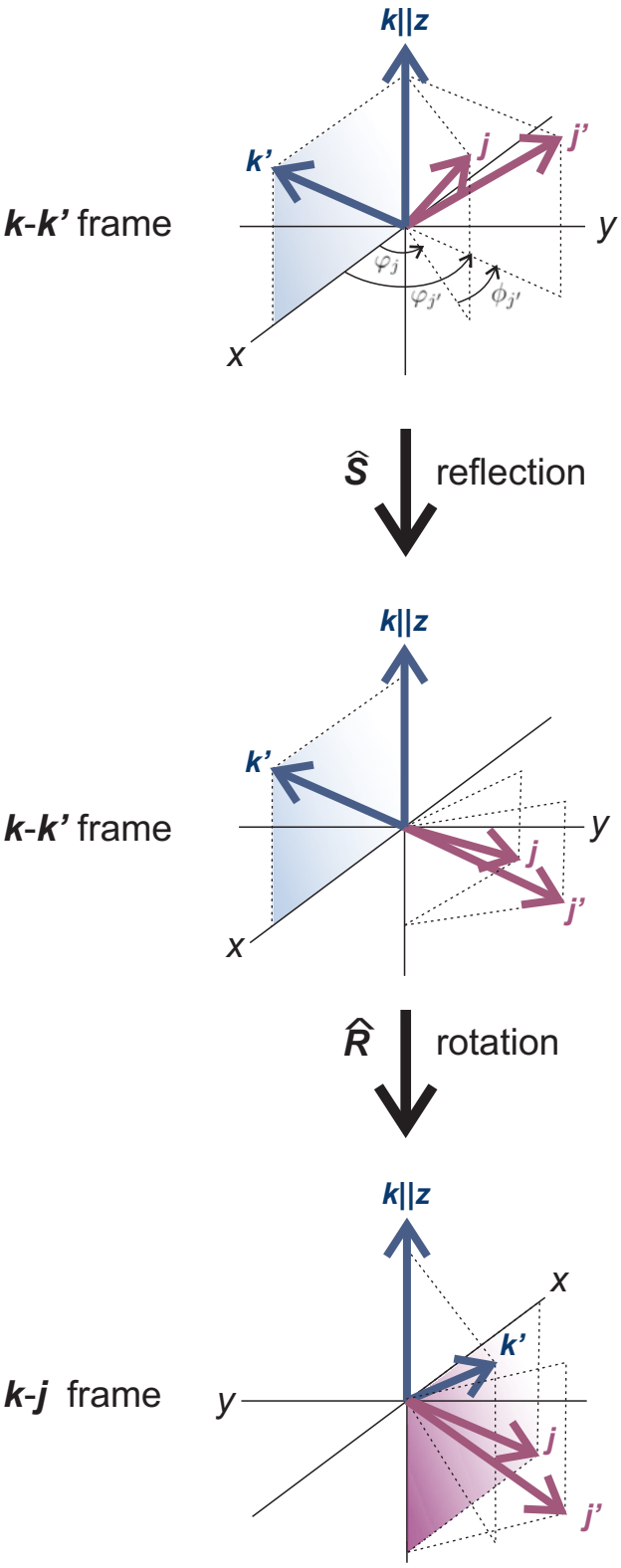
k||z
k'
j
j'
y
x
φ_j
$\varphi_{j'}$
$\phi_{j'}$
k-k' frame
$\hat{S}$
reflection
k||z
k'
y
j
j'
x
k-k' frame
$\hat{R}$
rotation
k||z
x
k'
y
j
j'
k-j frame

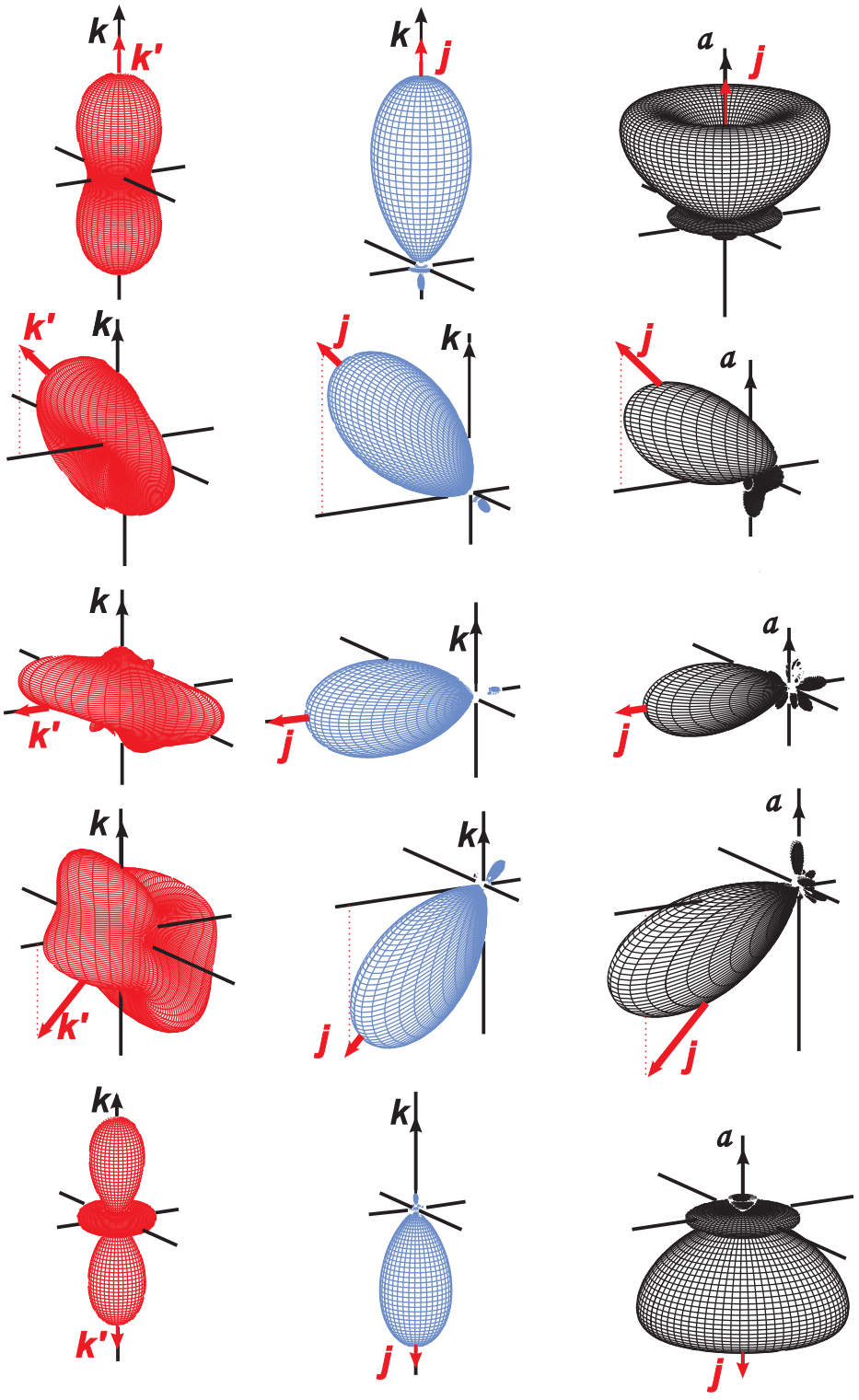
k
k'
k
j
a
j
k'
k
j
k
j
a
k
k'
k
j
j
a
k
k'
k
j
a
j

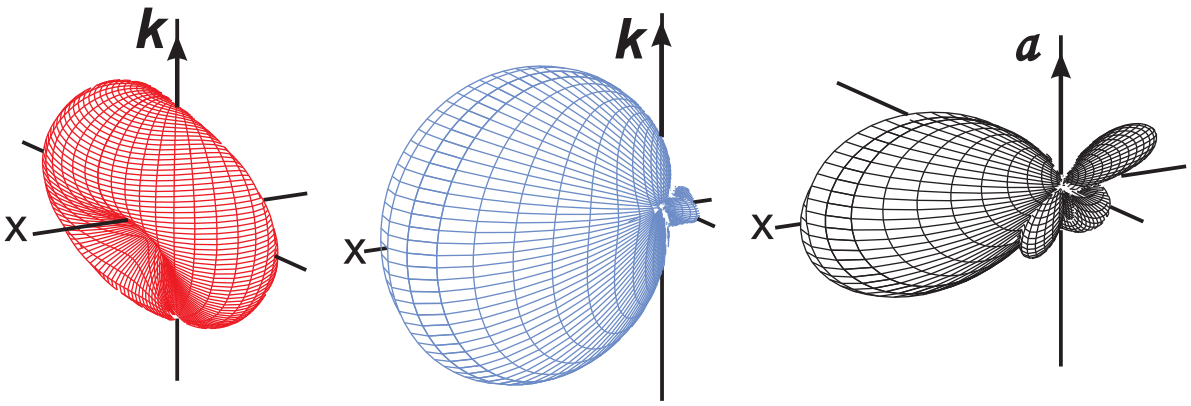
k
x
k
x
a
x

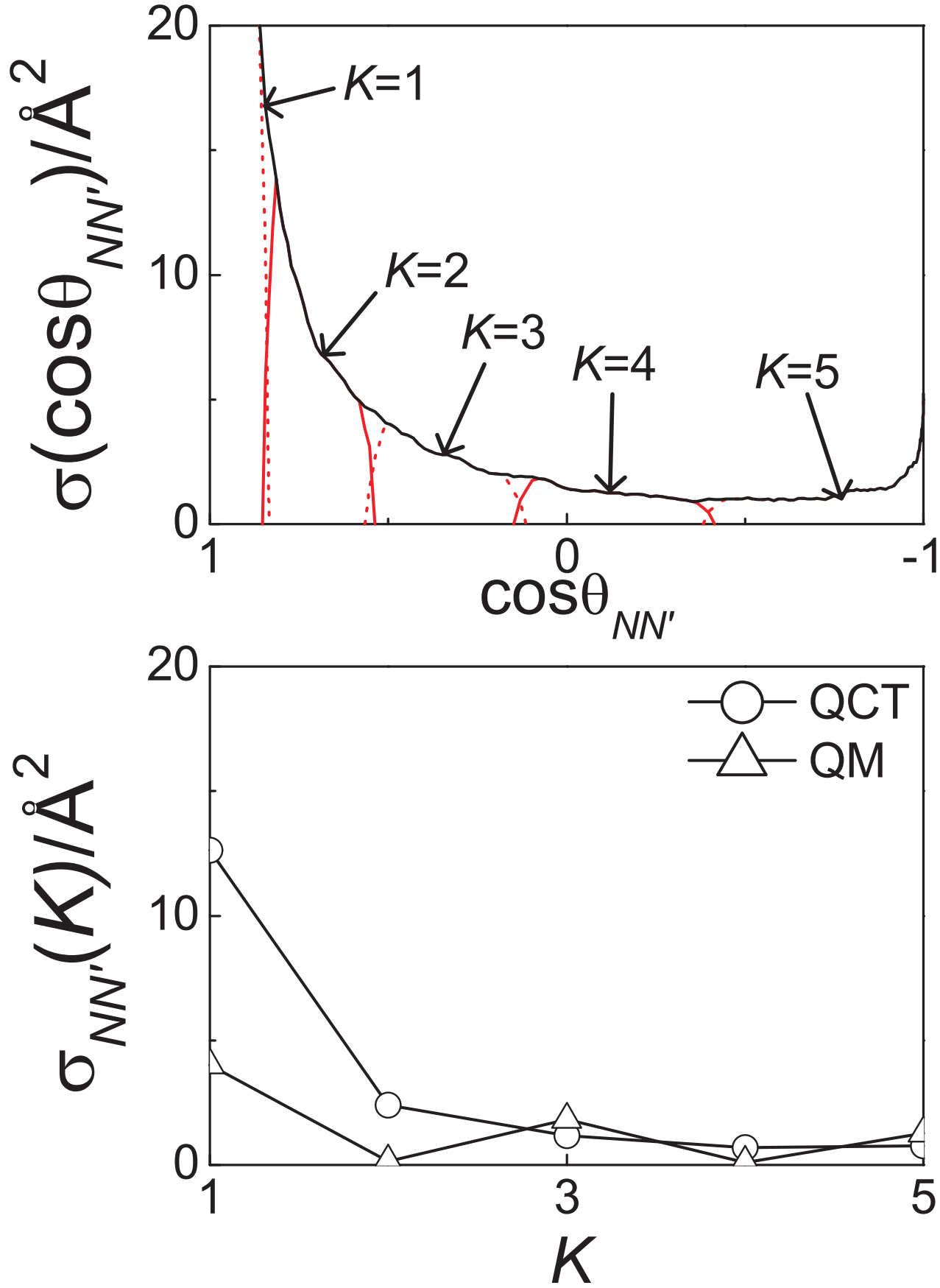
20
10
0
1
0
-1
$\sigma(\cos\theta_{NN'})/\text{Å}^2$
$\cos\theta_{NN'}$
K=1
K=2
K=3
K=4
K=5
20
10
0
1
3
5
$\sigma_{NN'}(K)/\text{Å}^2$
K
QCT
QM

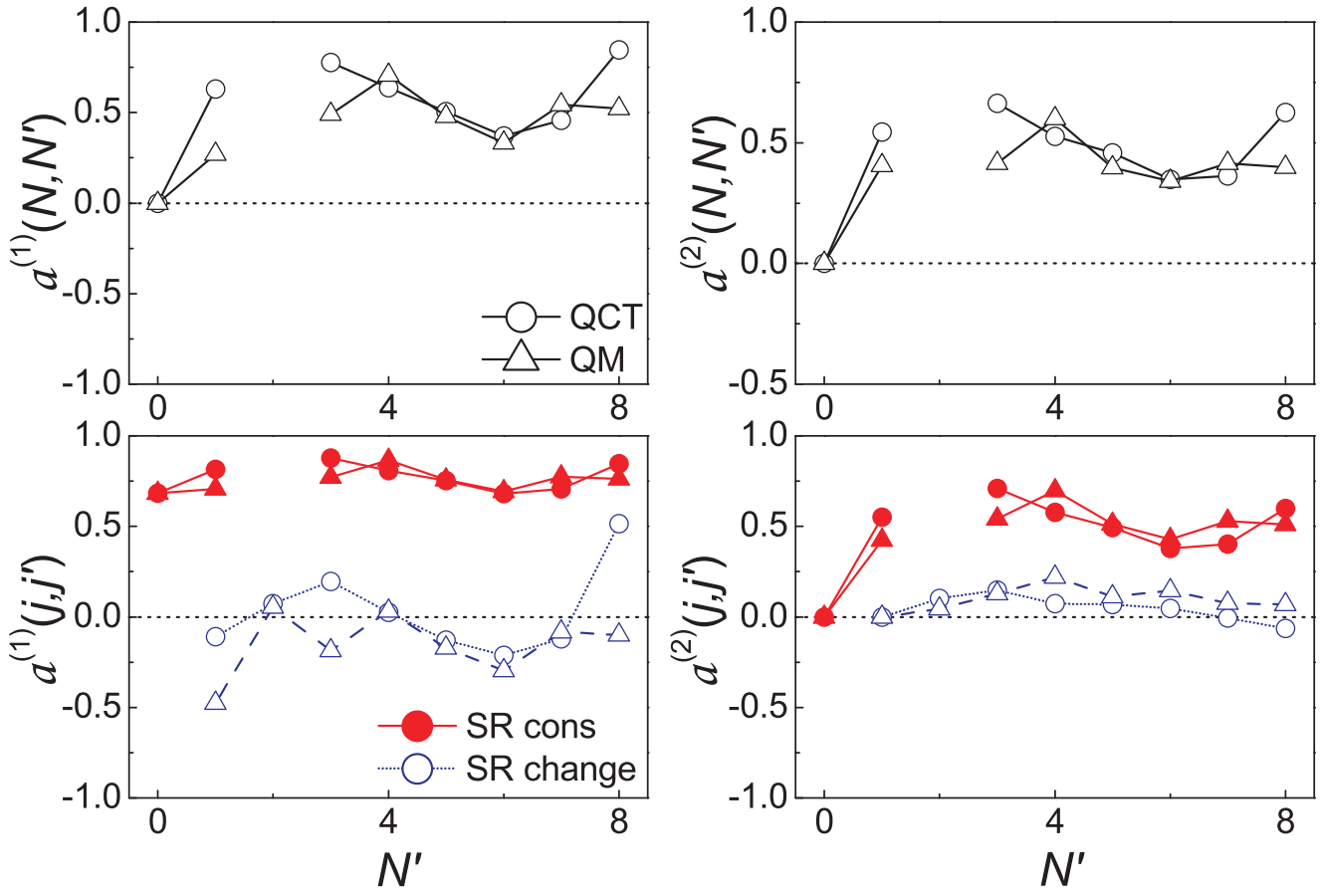
1.0
0.5
0.0
-0.5
-1.0
0
4
8
$a^{(1)}(N,N')$
$a^{(2)}(N,N')$
QCT
QM
$a^{(1)}(j,j')$
$a^{(2)}(j,j')$
SR cons
SR change
N'

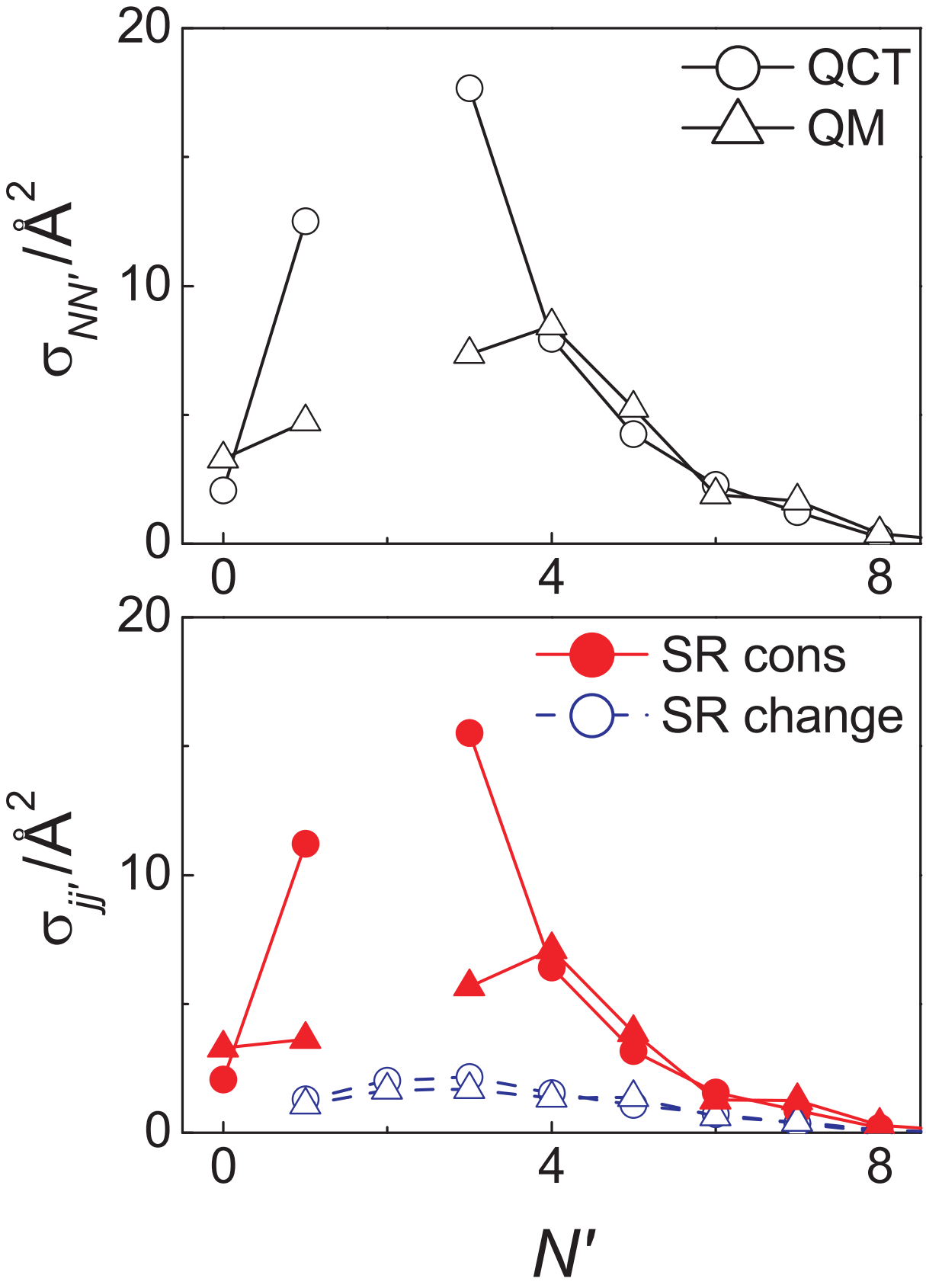
20
10
0
0
4
8
QCT
QM
$\sigma_{NN'}$/Å^2
SR cons
SR change
$\sigma_{jj'}$/Å^2
N'